Consiglio Nazionale delle Ricerche

COMES-NOSA

A finite element code for non-linear structural analysis

M. Lucchesi, C. Padovani, A. Pagni, G. Pasquinelli, N. Zani

Report CNUCE-B4-2000-003

Pisa

COMES-NOSA

A finite element code for non-linear structural analysis

M. Lucchesi, C. Padovani, G. Pasquinelli, A. Pagni, N. Zani

CNUCE – C.N.R. Via Vittorio Alfieri 1, 56010 Ghezzano Pisa, Italy

Report CNUCE-B4-2000-003

The finite element code NOSA (NOn-Linear Structural Analysis) has been developed by the *Mechanics of Materials and Structures* workgroup with the aim of testing new constitutive models for materials. It has moreover been applied to checking the algorithms used for integrating the equations of motion, as well as other numerical techniques for solving structural engineering problems.

The development of NOSA began in 1980 and has continued over the ensuing years along the research lines of the workgroup. In 1996, the CNUCE Institute became a member of the Multi-center Network for Computational Solid Mechanics (COMES). Since then, a large part of the group's development activities have been conducted within this framework, giving rise to the COMES-NOSA code.

The first version of the code included plane, three-dimensional and axisymmetric isoparametric elements [1] and allowed for elastic-plastic analyses in the presence of infinitesimal strains with the work-hardening models described in [2]. The code has subsequently been extended to include

cases of finite strains and contact problems, based on studies performed on both the constitutive equations [3, 4, 5, 6] and the methods for numerical integration of the equations of motion, in the presence of follower forces [7, 8, 9]. At the same time, an eight-node thin-shell element was added to the element library [10].

More recently, the constitutive equation for masonry-like materials has been added to the code with the purpose of studying the static of masonry solids and modelling restoration and reinforcement operations on constructions of particular architectural interest [11, 12, 13, 14, 15]. The code was then enhanced to be able to perform non-linear heat-conduction analysis on solids even in the non-stationary case, with boundary conditions concerning temperature and thermal fluxes. Today, the code allows for thermo-mechanical analysis of no-tension solids whose mechanical characteristics depend on temperature, in the presence of thermal loads [16, 17].

At the present, the development of the subroutines necessary for the dynamic analysis of masonry structures is in its final stage of completion.

Development of the code has been made possible through the funding of C.N.R. (progetto finalizzato Informatica, progetto finalizzato Materiali Speciali per Tecnologie Avanzate, progetto finalizzato Beni Culturali) and funding of the region of Tuscany (structural funds and Regional High Tech Network).

Over the past twenty years many engineering students at the University of Pisa have collaborated on the development of the code as part of their degree or doctorate thesis preparation.

The following table presents the flow-chart for COMES-NOSA relative to non-linear static analysis. The subsequent tables list, respectively, COMES-NOSA's elements library and the currently available constitutive laws.

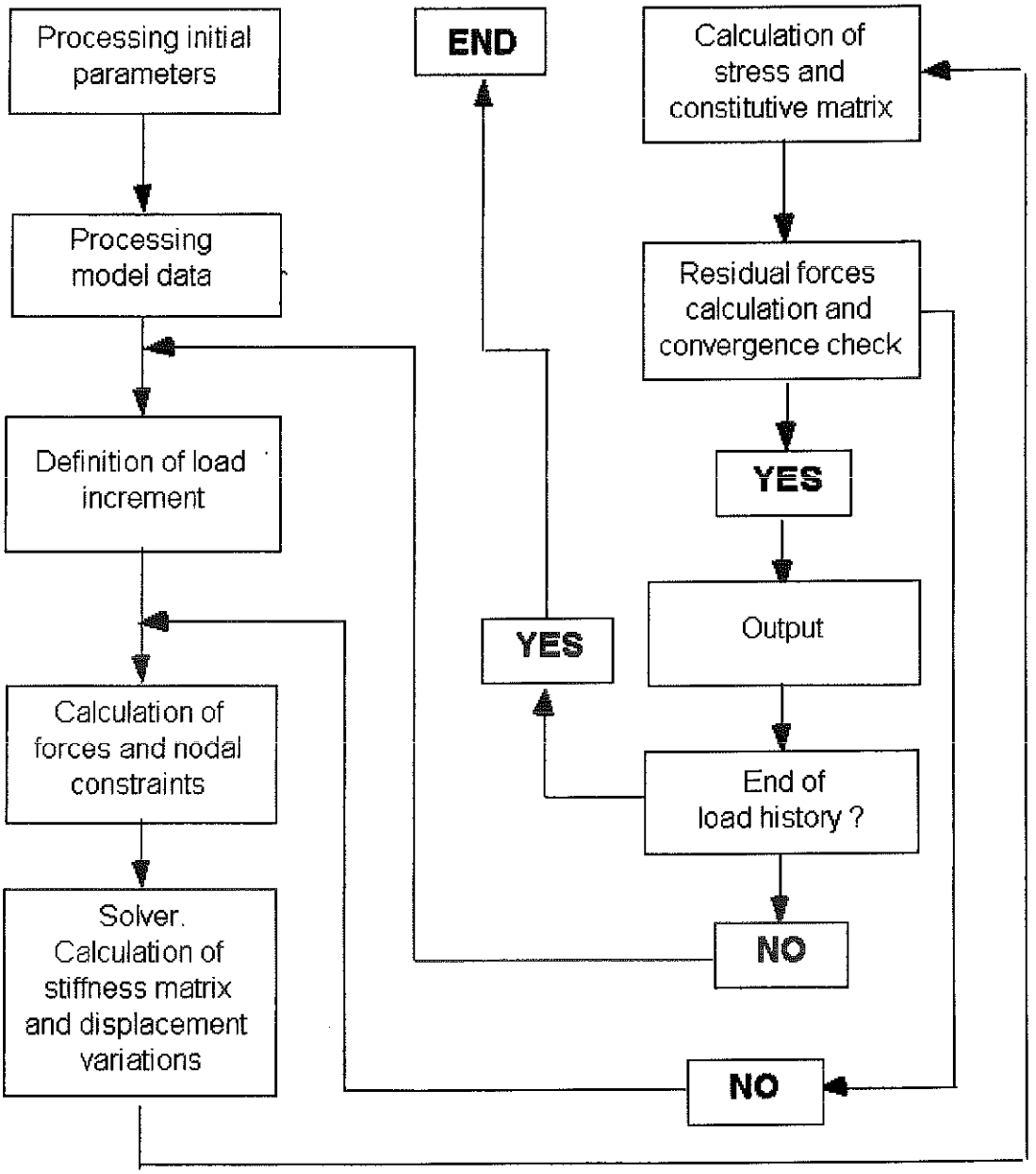
Processing initial parameters
Processing model data
Definition of load increment
Calculation of forces and nodal constraints
Solver. Calculation of stiffness matrix and displacement variations
END
YES
Calculation of stress and constitutive matrix
Residual forces calculation and convergence check
YES
Output
End of load history ?
NO
NO

Element library

Type	Interpolation	Degrees of freedom
Plane stress	8 nodes, quadratic	2 displacements
Plane strain	4 nodes, linear 8 nodes, quadratic	2 displacements
Axisymmetric	4 nodes, linear 8 nodes, quadratic	2 displacements
Three-dimensional	8 nodes, linear 20 nodes, quadratic	3 displacements
Thin shell	8 nodes, linear for displacements, quadratic for rotations	3 displacements at corner nodes +1 rotation in the mid-side nodes
Thick shell	4 nodes, linear	3 displacements + 3 rotations

Constitutive equations library

Linear elasticity	All types of elements
Elastoplasticity with small strain	All types of elements, but the shells
Elastoplasticity with finite strain	All elements with linear interpolation, but the shells
Material with zero tensile strength and infinite compressive strength	All type of elements
Material with zero tensile strength and bounded compressive strength	All type of elements

References

[1] HINTON E., OWEN D. R. J., Finite Element Programming, Academic Press, 1977.

[2] GUIDOTTI P, LUCCHESI M, PAGNI A., PASQUINELLI G., Elastic-Plastic Behaviour with Work Hardening: an Appropriate Model for Structural Software, *Meccanica* **19**, 1984.

[3] LUCCHESI M., PODIO GUIDUGLI P., Materials with Elastic Range: a Theory with a view toward Applications. Part I, *Arch. Rat. Mech. Anal.*, **102**, pp. 23-43, 1988.

[4] LUCCHESI M., PODIO GUIDUGLI P., Materials with Elastic Range: a Theory with a view toward Applications. Part II, *Arch. Rat. Mech. Anal.*, **110**, pp. 9-42, 1990.

[5] LUCCHESI M., OWEN D. R., PODIO GUIDUGLI P., Materials with Elastic Range: a Theory with a view toward Applications. Part III. Approximate Constitutive Relations, *Arch. Rat. Mech. Anal.*, **117**, pp. 53-96, 1992.

[6] LUCCHESI M., PODIO GUIDUGLI P., Materials with Elastic Range and the Possibility of Stress Oscillations in Pure Shear, Proc. Int. Conf. on Comp. Plasticity, Model, Software and Applications, Barcelona, 6-10 aprile 1987.

[7] GUIDOTTI P., LUCCHESI M., A Numerical Method for Solving Boundary-Value problems in Finite Plasticity, *Meccanica*, **23**, pp. 43-54, 1988.

[8] DEGL'INNOCENTI S., PADOVANI C., PASQUINELLI G., An improved numerical method to integrate the equation of motion in finite elastoplasticity problems, Complas II, Second International Conference on Computational Plasticity, Barcelona, September 1989.

[9] PASQUINELLI G., Simulation of Metal-Forming Processes by the Finite Element Method, *Int. J. Plasticity*, Vol. **11**, No. 5, pp. 623-651, 1995.

[10] GUIDOTTI P., LUCCHESI M., PAGNI A., PASQUINELLI G., Application of Shell Theory to Structural Problem Using the Finite Element Method, Quaderni de "La Ricerca Scientifica", **115**, 1986.

[11] LUCCHESI M., PADOVANI C. and PAGNI A., A numerical method for solving equilibrium problems of masonry-like solids. *Meccanica*, **24**, pp. 175-193, 1994.

[12] LUCCHESI M., PADOVANI C. and PASQUINELLI G., On the numerical solution of equilibrium problems of elastic solids with bounded tensile strength. *Comput. Methods Appl. Mech. Engrg.* **127**, pp. 37-56, 1995.

[13] LUCCHESI M., PADOVANI C. and ZANI N., Masonry-like materials with bounded compressive strength. *Int. J. Solids Structures* **33**, pp. 1961-1994, 1996.

[14] LUCCHESI M., PADOVANI C., PASQUINELLI G. and ZANI N., On the collapse of masonry arches. *Meccanica* **32**, pp. 327-346, 1997.

[15] LUCCHESI M., PADOVANI C., PASQUINELLI G. and ZANI N., The maximum modulus eccentricity surface for masonry vaults and limit analysis. *Mathematics and Mechanics of Solids* **4**, pp. 71-87, 1999.

[16] LUCCHESI M., PADOVANI C., PASQUINELLI G., Thermodynamics of no-tension materials. *Int. J. Solids and Structures* (to appear).

[17] PADOVANI C., PASQUINELLI G., ZANI N., A numerical method for solving equilibrium problems of no-tension solids subjected to thermal loads. *Comput. Methods Appl. Mech. Engrg.* (to appear).

Static analysis of elastic-plastic solids with COMES-NOSA

The COMES-NOSA code enables performing static analyses of elastic-plastic solids even in the presence of finite strains. The code permits the simulation of metal-forming processes, such as extrusion, deep drawing, etc. In particular, it is possible to solve the problem of the contact between a deformable body (the workpiece) and moving rigid surfaces (the dies). The algorithm implemented into COMES-NOSA for solving such a problem differs from the most commonly used methods in commercial codes in that:

1. The incremental equilibrium equation is calculated for the current configuration of the deformable body and thus given directly in terms of the Cauchy stress tensor.
2. The elastic-plastic constitutive response of the material is thoroughly described by an ordinary differential equation system where the yield condition is stated in the deformation space; so no prediction of the increase in stress is needed. Moreover, the system is numerically integrated, taking, as initial conditions, those at the beginning of the load increment: in this way the artificial unloading that may be produced by stress redistribution in a high stress-gradient zone or by the motion of the node in establishing the right contact conditions is avoided.
3. The contact algorithm is based on direct application of boundary conditions, i. e., an automatic procedure has been set up that translates, at each iteration, the contact conditions between the workpiece and rigid dies into the appropriate conditions applied to the boundary nodes.

As an example, two applications of the contact algorithm implemented into COMES-NOSA, are described. The first example concerns a bulge test carried out at CSM (Centro Sviluppo Materiali). Subsequently, we shall analyse a case of deep drawing performed at the Fiat Research Centre. For both cases experimental data is available.

Bulge test

The test concerns a thin steel disk, clamped along its boundary by a draw-bead between the blankholder and die and subjected to pressure on one face. During its motion the disk rests on a bearing which has a quarter-circle cross-section.

The geometrical and mechanical data are the following

Radius of the disk at the draw-bead level	132 mm,
Radius of the pressurised part	86 mm,
Radius of the bearing section	11 mm,
Thickness of the disk	0.8 mm,
Maximum pressure	7.4 MPa,
Young's modulus	$2.1\ 10^5$ MPa,
Poisson's ratio	0.3.

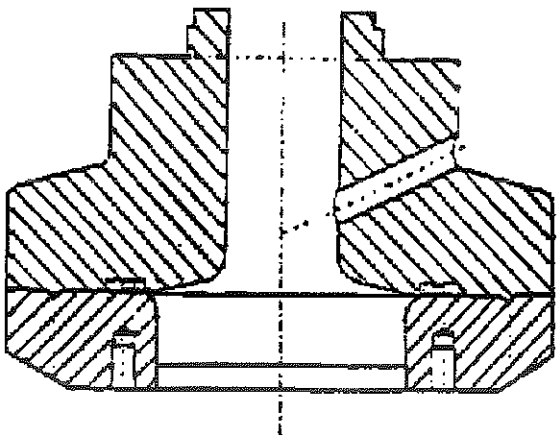

Figure 1. Bulge test apparatus.

Figure 1 shows a sketch of the experimental apparatus. The disk is made of high-strength steel. Due to the lamination process, the material exhibits a certain amount of in-plane anisotropy which has been neglected (nothing is known about the direction along the thickness). Several simulations have been performed by considering both isotropic and kinematic hardening and using the hardening curves shown in figure 2.

The disk has been discretised with 138 axisymmetric four-node elements (two elements within the thickness), and each run has required 196 load increments to reach the maximum pressure, and 85 increments to unload to zero pressure. The results obtained in purely isotropic hardening are summarised in figures 3, 4, 5, 6 and 7. Figure 3 shows the final configuration of a disk section as compared to its initial one. In figure 4 the axial displacements of the points of the symmetry axis are plotted as a function of the pressure (the horizontal parts represent the unloading path). Figure 5 presents the final thickness of the sheet as a function of the undeformed radial distance. Lastly, the final meridional strain is plotted in figure 6 vs. the initial radial distance, while figure 7 shows the final circumferential strain vs. the radial distance.

The uncertainty in the experimental data in figures 6 and 7 is twice the measured standard deviation, and the strains have been averaged over the thickness.

The discrepancy between the numerical results and experimental data can be explained by the fact that, with the constitutive law we have adopted, the material response is too stiff at low strain levels (below 0.1). In fact, from figure 4, we can see that at low pressure the calculated displacement of the central point is much lower than the measured one, whereas in correspondence of higher values of pressures the calculated and measured displacements coincide. Moreover, behaviour that is too stiff at low strain implies underestimation of the final strains in the disk's external part and overestimation in its central part, as can be seen from figures 5-7. In order to attain good agreement between numerical and experimental data, without changing the constitutive law, we have used another hardening curve, that indicated in figure 2 as 'modified curve': it is similar to the curve of a mild, rather than high-strength steel. In fact, as can be seen in the figures, very satisfactory results are obtained by adopting this modified curve.

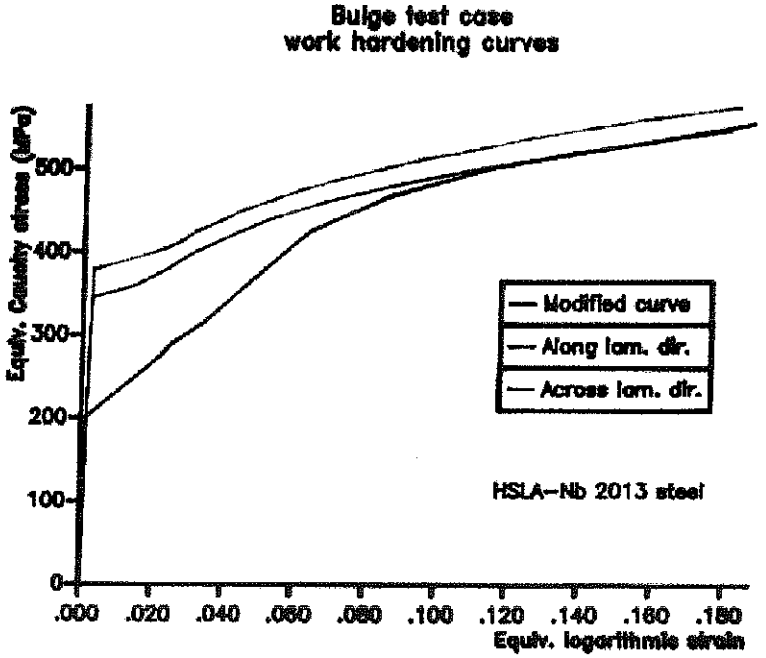

Figure 2. Work-hardening curves.

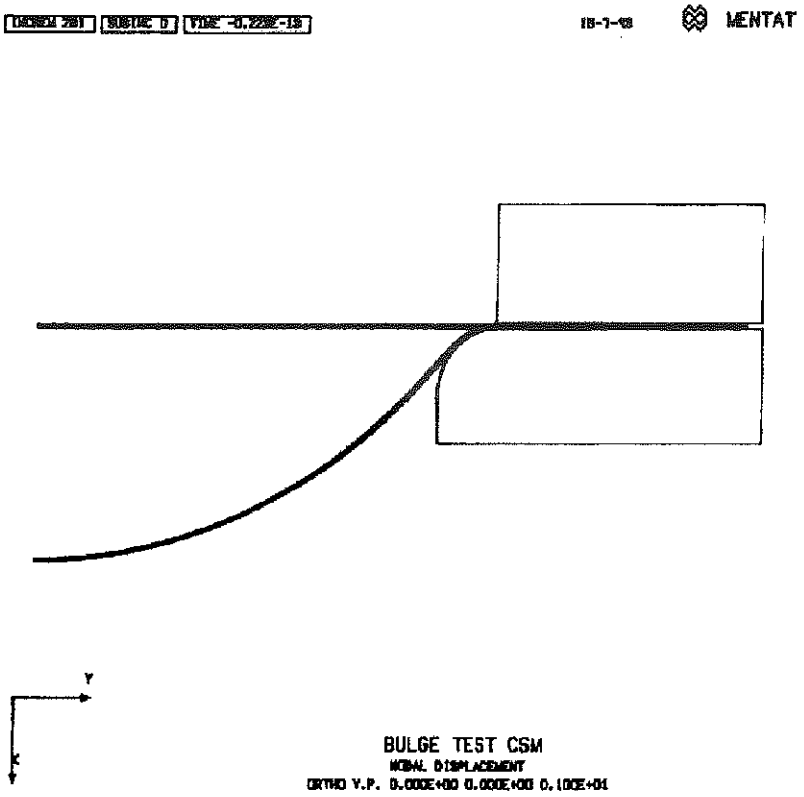

Figure 3. Disk final configuration.

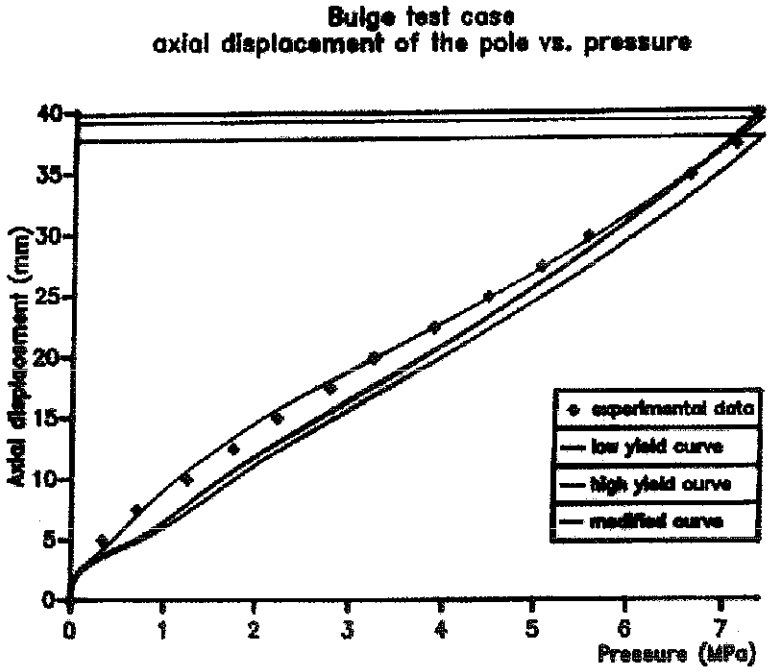

Figure 4. Axial displacement vs. pressure.

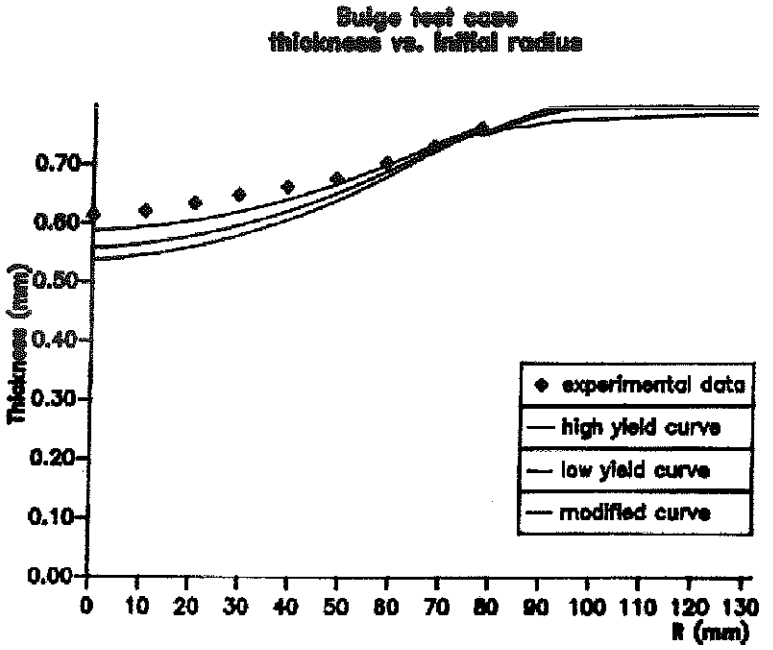

Figure 5. Thickness vs. radial distance.

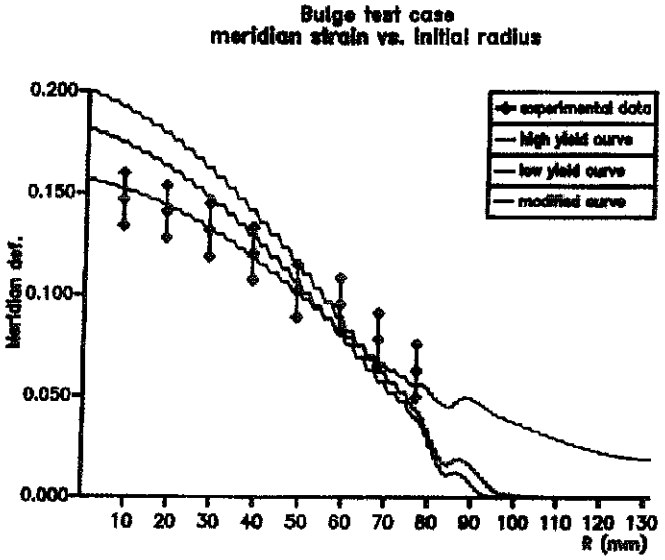

Figure 6. Meridional strain vs. radial distance.

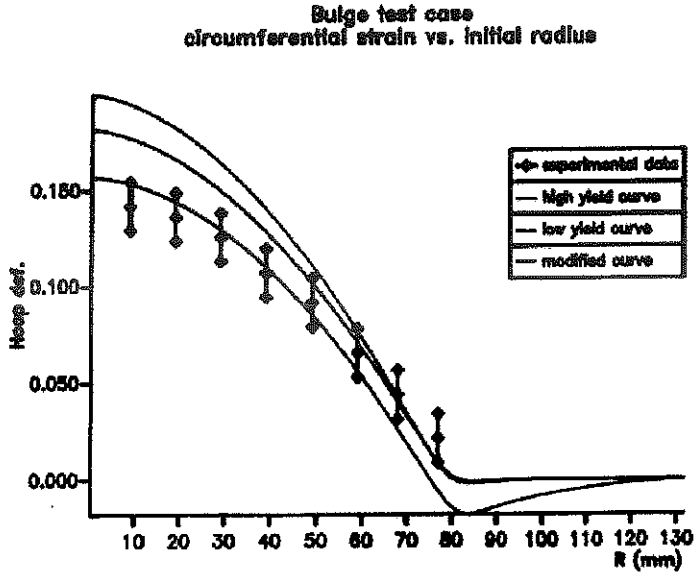

Figure 7. Circumferential strain vs. radial distance.

Bibliography

[1] Pasquinelli G., Simulation of metal-forming processes by the finite element method. *Int. Journal of Plasticity*, **11** (5), pp. 623-651, 1995.

A deep-drawing case

In order to check the performance of the contact and friction algorithm, we chose an axisymmetric deep-drawing trial carried out at the Fiat Research Center, for which the experimental data is available. The test case deals with a disk of $FePO_4$ steel pushed by a cylindrical punch with a double curvature head: the total displacement of the punch is 65 mm. The experimental set-up is shown in figure 8 and the material's work-hardening curve is plotted in figure 9: the curve represents an interpolation of the experimental values obtained from uniaxial tests on standard specimens cut at different angles to the lamination direction. The disk was discretised with 158 axisymmetric four-node elements (two elements within the thickness); the mesh is finer near the die in order to obtain better modelling of the contact conditions. Because the use of a fixed-force blankholder is not yet provided for by COMES-NOSA, a fixed blankholder was used and, to avoid ironing of the sheet, an initial gap of 0.5 mm was allowed between blankholder and sheet. Moreover, a similar gap in addition to the sheet thickness, was left between the die and punch. From figure 10, where the final configuration of the disk is compared with the initial configuration, it can be seen that the sheet losses contact with the blankholder and comes to rest on the die alone. In figure 11 the axial reaction force on the punch, calculated for different values of the Coulombian friction coefficient, is plotted as a function of punch displacement and compared with the experimental results. We can see that the best results are obtained for the friction coefficient 0.2. Moreover, as expected, the maximum value of the force on the punch moves towards higher displacements when a higher value is used for the friction coefficient.

Bearing in mind the arguments set forth in the previous example, it seems that the constitutive law adopted can more realistically model the response of a material such as the mild steel used in this case than that of the high-strength steel used in the bulge test.

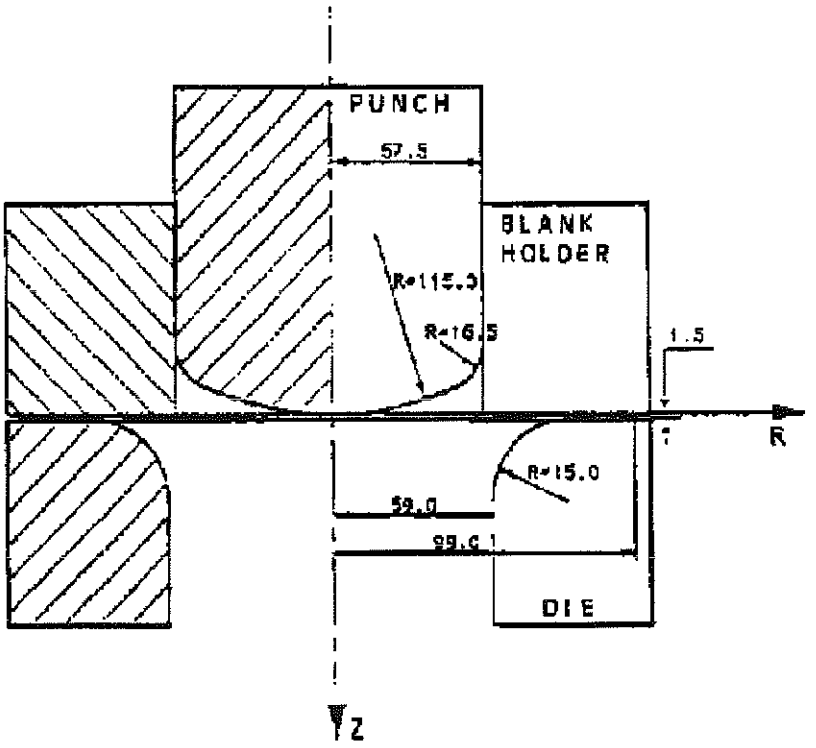

Figure 8. Experimental set-up.

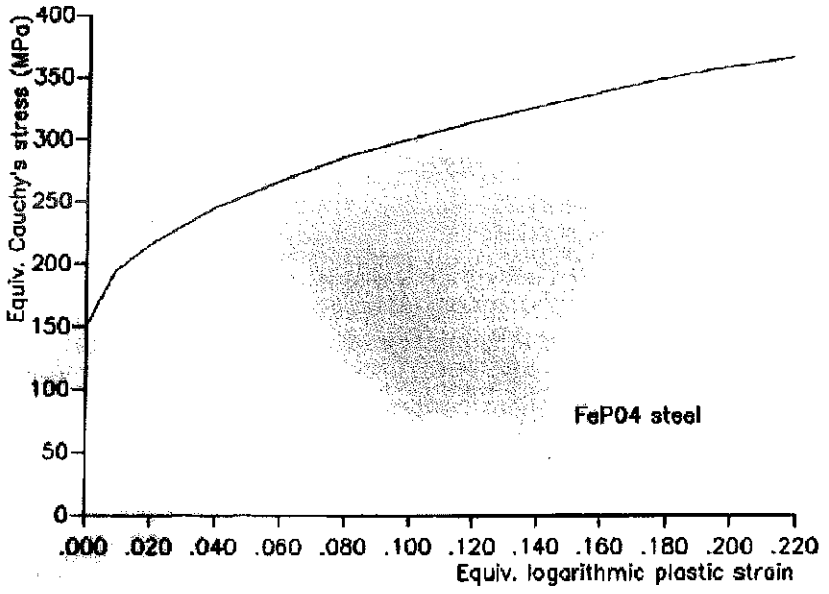

Figure 9. Work-hardening curve.

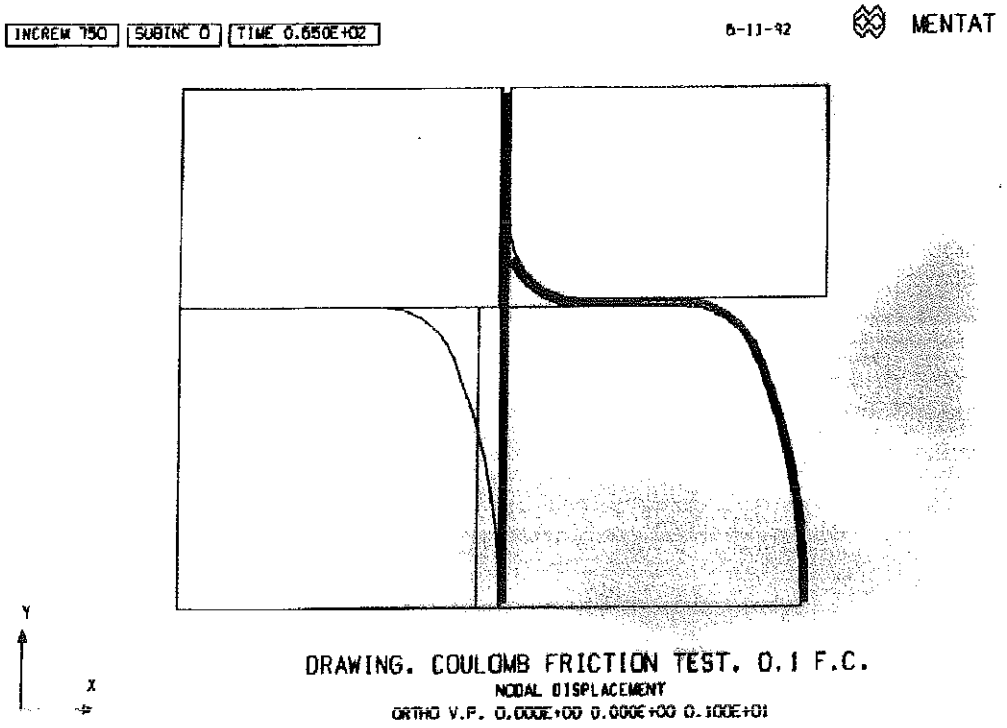

Figure 10. Final configuration.

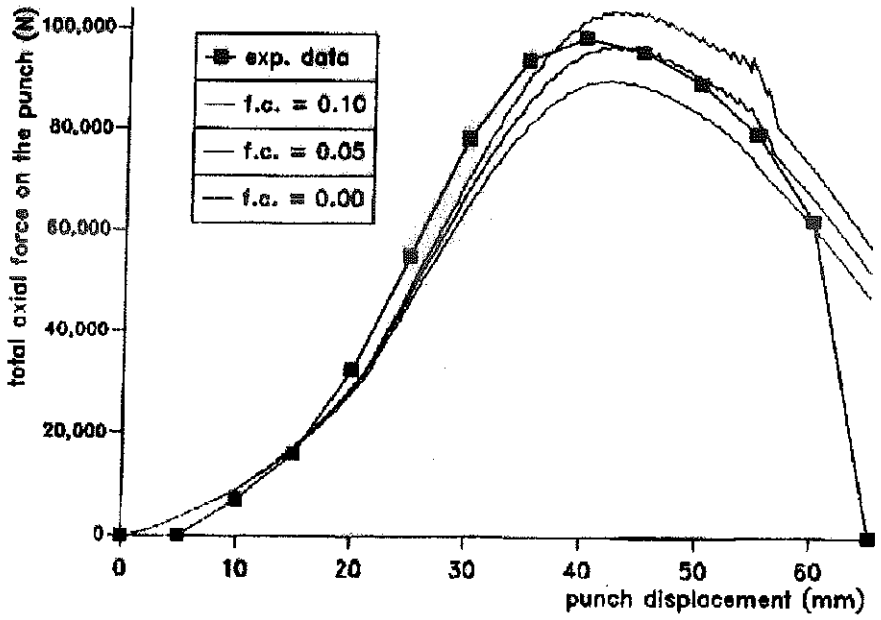

Figure 11. Punch force vs. displacement.

Bibliography

[1] Pasquinelli G., Simulation of metal-forming processes by the finite element method. *Int. Journal of Plasticity*, **11** (5), pp. 623-651, 1995.

Static analysis of masonry structures with COMES-NOSA

Although masonry has been used in building for centuries, it is only in recent years that constitutive models and calculation techniques have been available that enable realistic description of the static behaviour of structures made of this anisotropic, heterogeneous material whose response to tension is fundamentally different from that to compression.

Until a century ago all consolidation work on historical buildings was based exclusively on considerations of an empirical nature. The advent of the industrial revolution and the ever-increasing dominance of constructions in iron have rendered the mathematical theory of the elasticity a formidable tool for the design and checking of metal structures. The success attained in applying linear-elastic calculations to such structures elicited so much enthusiasm that the models sometimes came to be employed in a rather arbitrary fashion to the study of masonry constructions as well. On the one hand, this has hampered research efforts to further the work begun in 18th Century on developing proper calculation techniques for masonry structures, while on the other, it has contributed to breeding scepticism regarding the very possibility of modelling the static behaviour of masonry buildings. For many years the fundamental studies on materials not withstanding tension, begun in the 1920s, remained without practical application, and some technicians operating in the field of restoration still hold linear-elastic analysis to be the main tool at their disposal. Such an attitude has been further aggravated by the great complexity of all constitutive equations studied for modelling the behaviour of masonry, which thus makes it extremely arduous to determine explicit solutions for the equilibrium problems encountered in reality. In fact, the first applications were developed only in the sixties and were restricted to limit analysis of relatively simple masonry structures.

Recently, the availability of ever more powerful computers and sophisticated numerical techniques for solving non-linear problems has reopened the debate on the possibility and opportuneness of modelling restorative work on historical building with the aim of evaluating its effects on the structures' static before its implementation. Recent studies have led to a better understanding of the constitutive equation of no-tension materials and the development of suitable numerical techniques that have allowed its application to calculations of masonry structures.

The constitutive equation studied by the CNUCE workgroup on *Mechanics of Materials and Structures* is based on the hypothesis that masonry is a non-linear isotropic material, having low tensile strength and bounded compressive strength. More precisely, we assume that the

infinitesimal strain $\mathbf{E}$ is the sum of three parts: an elastic part $\mathbf{E}^e$ on which the Cauchy stress tensor $\mathbf{T}$ depends linearly and isotropically, a positive semi-definite fracture strain $\mathbf{E}^t$ and a negative semi-definite crushing strain $\mathbf{E}^c$,

$$\mathbf{E} = \mathbf{E}^e + \mathbf{E}^t + \mathbf{E}^c, \tag{1}$$

$$\mathbf{E}^t \in \mathrm{Sym}^+, \ \mathbf{E}^c \in \mathrm{Sym}^-, \ \mathbf{E}^t \cdot \mathbf{E}^c = 0. \tag{2}$$

$$\mathbf{T} = \mathbb{C}[\mathbf{E}^e], \tag{3}$$

where $\mathbb{C}$ is the positive definite symmetric forth-order tensor $\mathbb{C} = 2\mu\mathbb{I} + \lambda\mathbf{I}\otimes\mathbf{I}$, with μ and λ the material's Lamé moduli. $\mathbb{I}$ is the fourth-order identity tensor and $\mathbf{I}\otimes\mathbf{I}[\mathbf{A}]=(\mathrm{tr}\mathbf{A})\mathbf{I}$, for every tensor $\mathbf{A}$, with $\mathbf{I}$ identity tensor. In (2) Sym^+ and Sym^- denote the sets of all positive semi-definite and negative semi-definite symmetric tensors, respectively.

Moreover, we assume that the eigenvalues of the stress belong to the interval $[-\sigma^t, \sigma^c]$ in which the quantities σ^c and σ^t depend on the material and indicated the maximum resistance respectively, to compression and traction, respectively

$$\mathbf{T} - \sigma^t\mathbf{I} \in \mathrm{Sym}^-, \quad \mathbf{T} + \sigma^c\mathbf{I} \in \mathrm{Sym}^+. \tag{4}$$

Finally, we suppose that certain orthogonality conditions between fracture and crushing strains and the stress tensor hold,

$$(\mathbf{T} - \sigma^t\mathbf{I}) \cdot \mathbf{E}^t = 0, \quad (\mathbf{T} + \sigma^c\mathbf{I}) \cdot \mathbf{E}^c = 0. \tag{5}$$

For $\sigma^t = 0$ and $\sigma^c = \infty$, we arrive at the classical masonry-like material, non-resistant to tension and infinitely resistant to compression, for which no crushing strain occurs and the fracture strain is orthogonal to the stress.

The main properties of the constitutive equation have been investigated and proved, and solutions for the two and three-dimensional problems have been explicitly calculated.

Despite the relative simplicity of this constitutive equation, determining the explicit solution to equilibrium problems of any practical interest is nonetheless very difficult. Therefore, in order to study real problems it is necessary to resort to numerical methods, particularly, the finite element method. To this end, opportune numerical techniques have been developed. They are based on the Newton-Raphson method for solving the non-linear system obtained through discretising the structure into finite elements. Their application requires that the derivative of the stress with respect to the strain be explicitly known, as this is needed in order to calculate the tangent stiffness matrix.

The numerical method studied at CNUCE has therefore been implemented into the finite element code COMES-NOSA which allows determination of the stress state and the presence of any cracking, and moreover enables modelling to be performed of any potential consolidation and restoration work, such as, for example, the fitting of chains.

The examples reported in the following, some of which were commissioned to the *Mechanics of Materials and Structures* workgroup by public agencies, serve to highlight the potentials of COMES-NOSA in real applications.

The Baptistery of Volterra cathedral

The Romanesque Baptistery in Volterra, dating from the 10th century, has an octagonal floor plan (figures 12 and 13). The current dome crowning the Baptistery is not the original roof; it was constructed in about 1427. It is brick masonry of thickness varying from 0.6 m at the keystone to 0.9 m at the springing. Over the years, the Baptistery has suffered cracking on the dome vault as well as on the walls of the octagon. These latter have consequently risen by 2.75 m. In 1930 restoration and reinforcement was carried out, which included, amongst other measures, the application to the cupola of two chains, respectively, of cross-section 4x7 cm^2 and 3x6 cm^2, at distances of 1.2 m (chain 1) and 3.4 m (chain 2) from the springing (figure 14). Another chain was placed on the octagon walls just above the upper row of windows (chain 3). The positioning of the chains was decided upon by considering the material to be linear elastic and applying the calculation procedure proposed by Camillo Guidi in 1913. More precisely, a 22.5° wedge of arch was considered and subdivided into 13 blocks, each 1.2 m in length. It was assumed that the normal force to the lateral face of the blocks was exerted upon the barycenters of the block faces themselves. Furthermore, the line of thrust was constrained to pass through the barycenters of all blocks. Using this procedure, it was deduced that the circumferential compressive force increased from the crown down to a certain height, after which it decreases to zero at parallel at 24° from the springing plane. It was therefore decided to chain the cupola at the same parallel and place another near the springing.

In 1995 the Baptistery underwent restoration work which included refacing of the vault's roofing, as it has been damaged by rainwater seepage. At the request of the Monuments and Tunnels Authority of Pisa, Livorno, Lucca and Massa Carrara, the Baptistery has been studied by means of the COMES-NOSA code, under the assumption that the material does not support tension. A quarter of the monument has been discretised by using 3387 shell elements (figure 15); the analysis has been conducted in two stages. In the first stage, the cupola is subjected to its own weight. Figure 16 shows the deformed configuration as compared to the initial one: it is evident that the thrust of the cupola on the springing wall causes meridian cracking, as has been found in reality. In the second stage, the three metallic chains are activated, tensed by means of cooling by 75°C (carried out in 8 increments) and constrained to follow the masonry structure's displacements in the direction normal to it. Figure 17 shows the deformed configuration

corresponding to chain cooling equal to 60° C. The compacting of the structure due to the action of the reinforcement ringing is evident.

Figures 18, 19, 20 and 21 show the line of thrust along a vault rib without chains and with them at different tension values. Figures 19, 20 and 21 refer to chain cooling of 25° C (case I), 50° (case II) and 75° C (case III), respectively. The tension values in the chain are

Case I

$N = 13500$ N (chain 1)

$N = 14500$ N (chain 2)

$N = 25000$ N (chain 3);

Case II

$N = 43000$ N (chain 1)

$N = 46000$ N (chain 2)

$N = 59000$ N (chain 3);

Case III

$N = 99000$ N (chain 1)

$N = 106000$ N (chain 2)

$N = 113000$ N (chain 3).

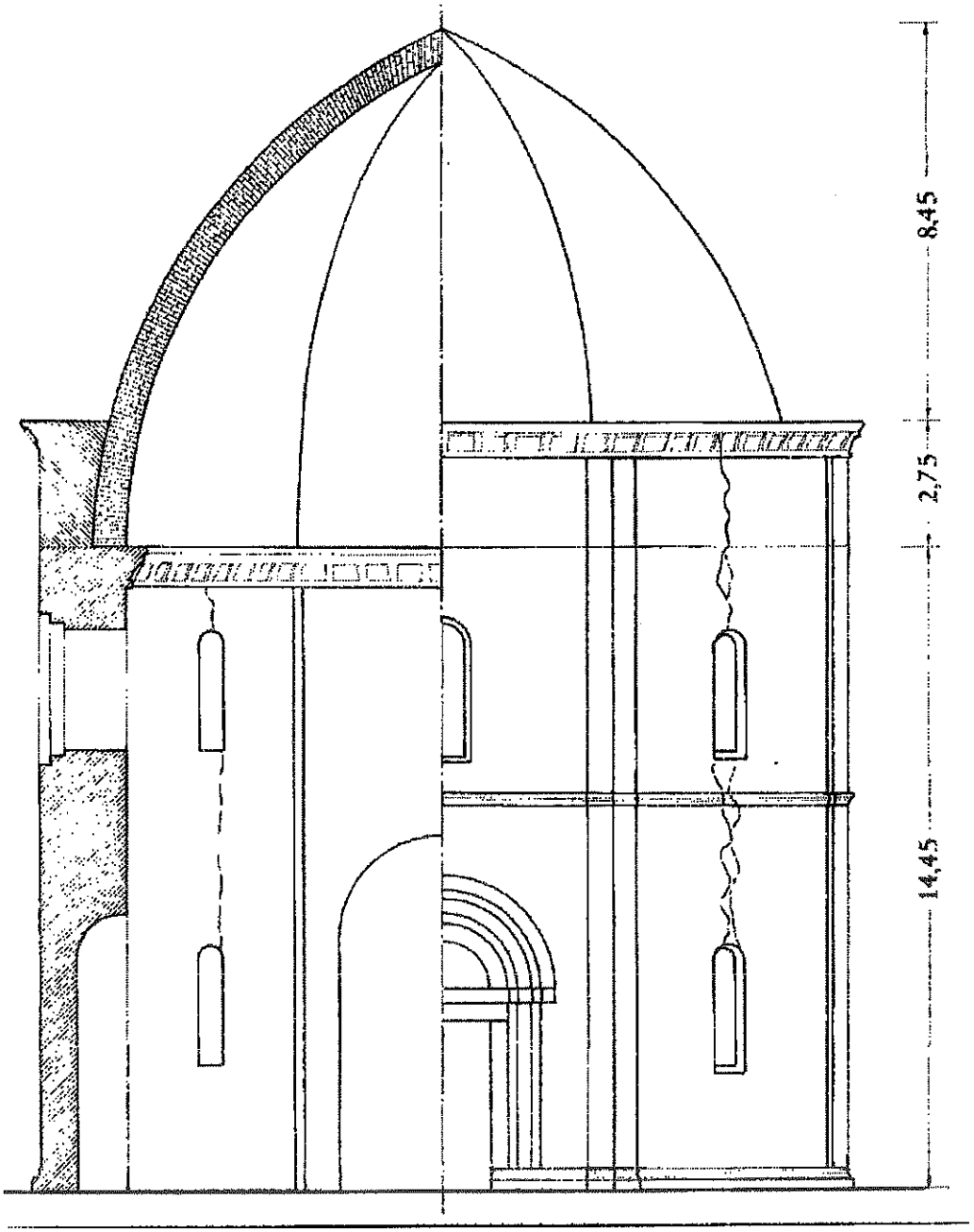

Figure 12. View of the Baptistery.

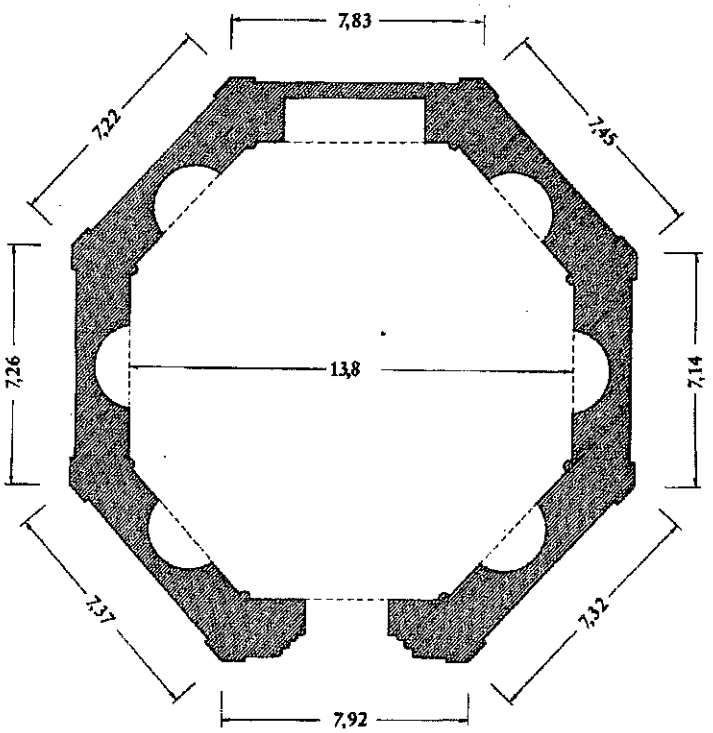

Figure 13. Baptistery floor-plan.

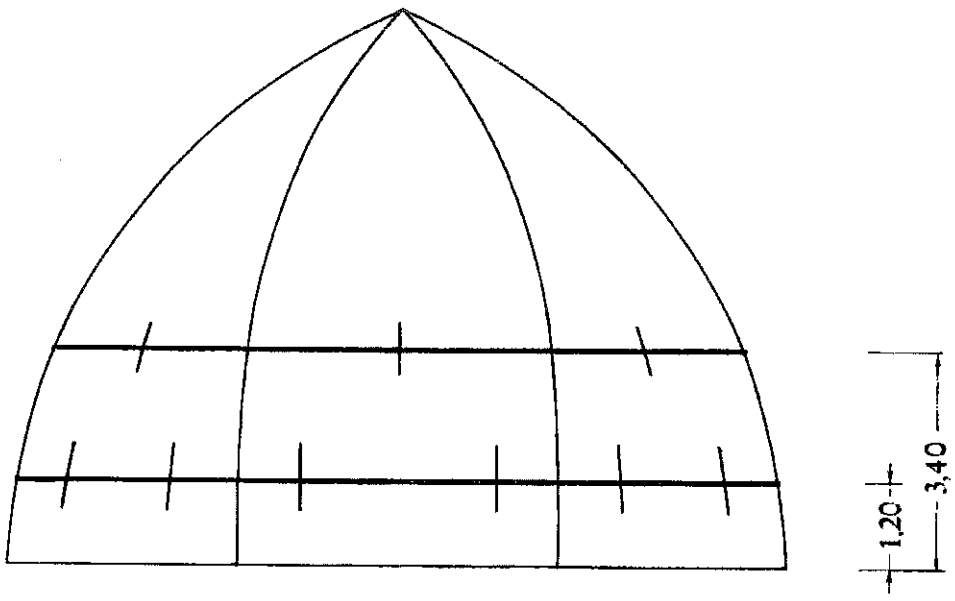

Figure 14. View of the Baptistery vault with chains.

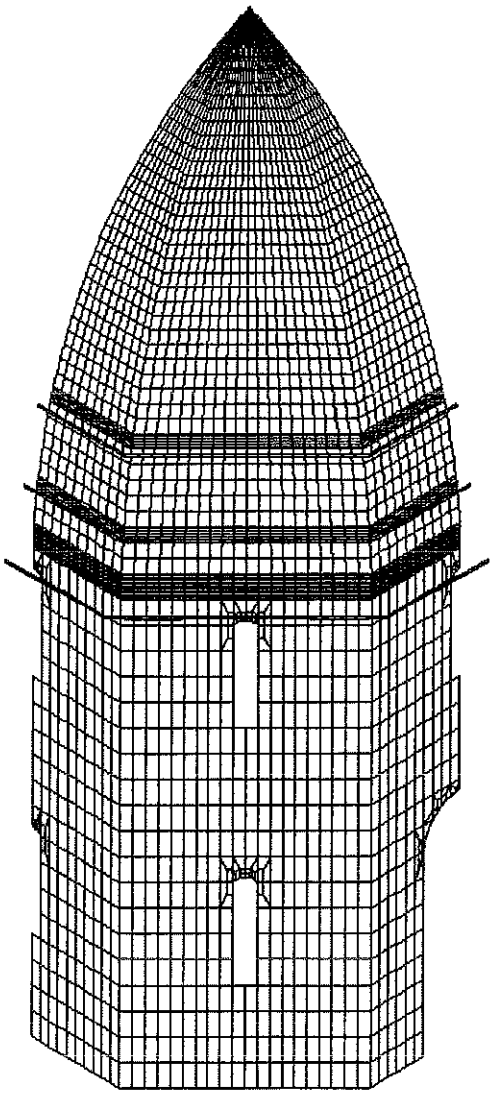

Figure 15. Finite element mesh.

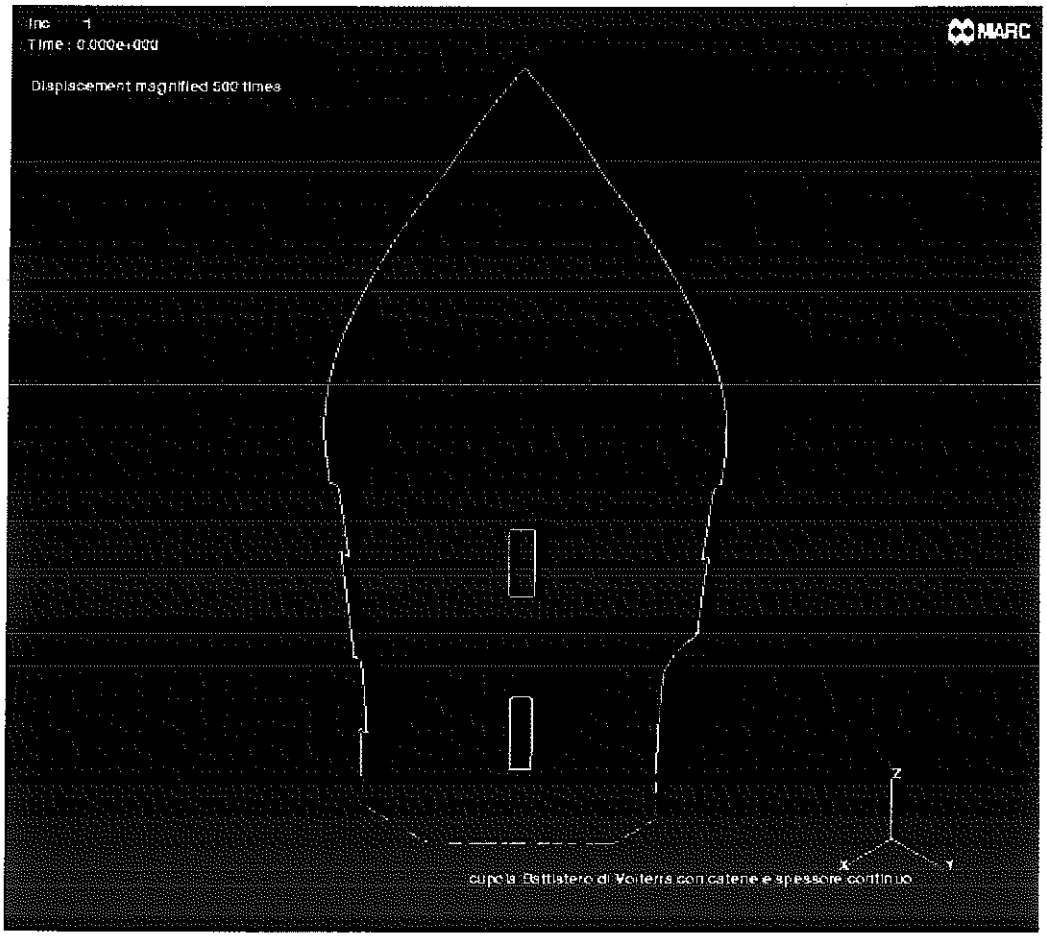

Figure 16. Deformed configuration without chains.

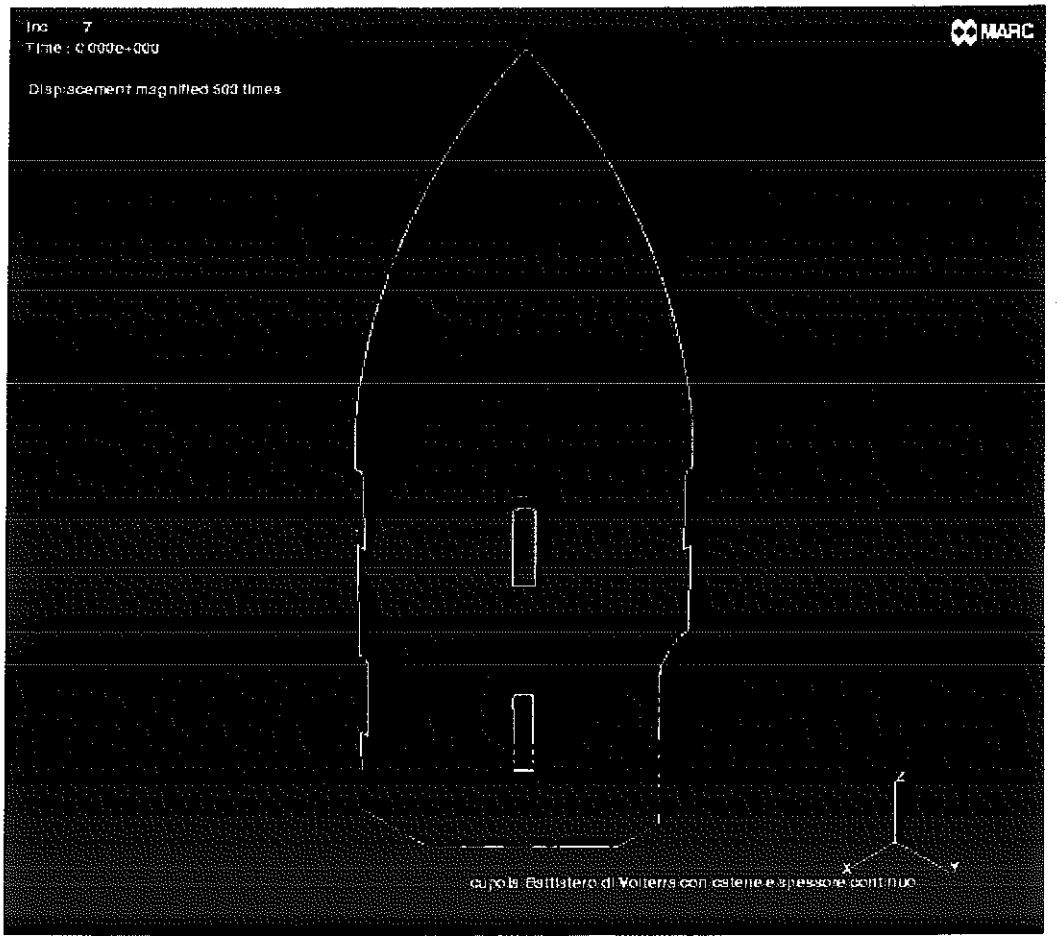

Figure 17. Deformed configuration with chains.

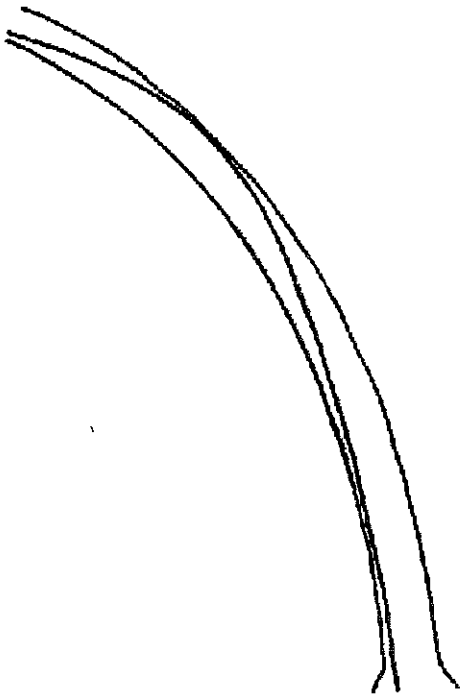

Figure 18. Line of thrust in a vault rib in the absence of chains.

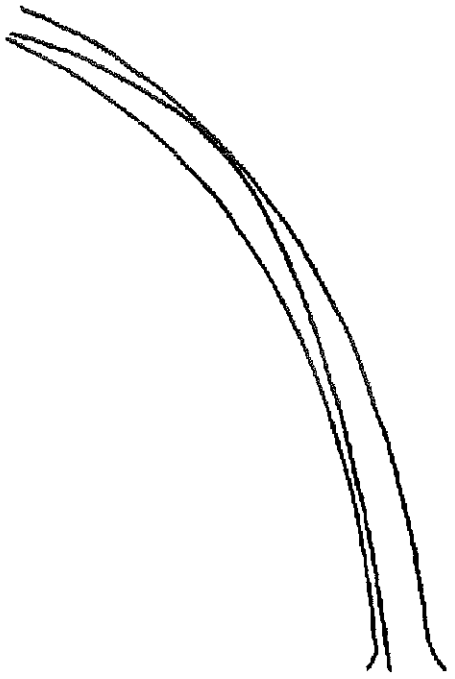

Figure 19. Line of thrust in a vault rib in presence of chains (case I).

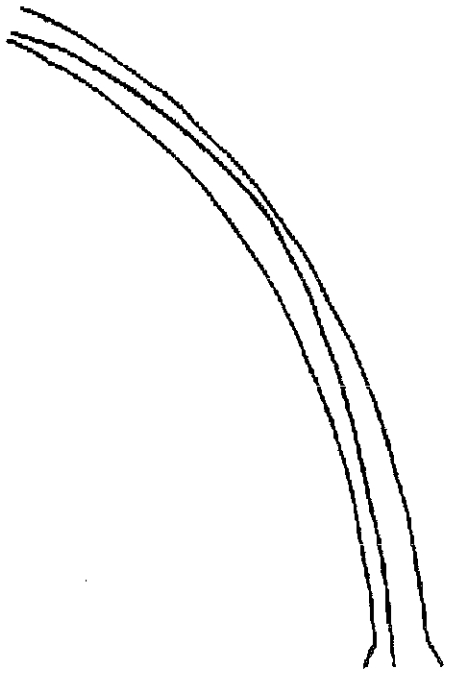

Figure 20. Line of thrust in a vault rib in the presence of chains (case II).

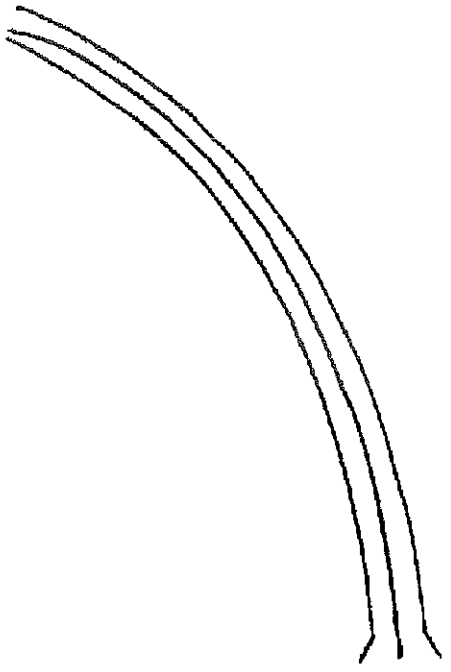

Figure 21. Line of thrust in a vault rib in the presence of chains (case III).

Bibliography

[1] Leoncini G. Illustrazione sulla cattedrale di Volterra. Tipografia sordo-muti di Luigi Lazzeri (1869).

[2] Guidi C. Lezioni sulla scienza delle costruzioni. Politecnico di Torino (1913).

[3] Lucchesi M., Padovani C., Pasquinelli G, Zani N. A numerical method for masonry vaults. Internal Report CNUCE C95-25 (1995).

[4] Lucchesi M., Padovani C., Pasquinelli G, Zani N. "Un metodo numerico per la soluzione del problema di equilibrio delle volte in muratura". *Atti del XII Congresso Nazionale dell'Associazione Italiana di Meccanica Teorica e Applicata*, Napoli, Castel dell'Ovo, 3-4-5-6 Ottobre 1995, Meccanica delle Strutture Tomo 1, pp. 199-204.

[5] Pasquinelli G. Un esempio di modellazione degli anelli di rinforzo nelle costruzioni in muratura: la cupola del battistero del duomo di Volterra. Conferenza MARC 22-23 maggio 1997 Starhotel President Corte Lambruschini 4 Genova.

The Mosca bridge in Turin

The Mosca bridge over the Doria Riparia river in Turin was constructed in 1827. It consists of 93 voussoirs made of Malanaggio granite, has a span of 45 m, an intrados rise of 5.5 m and thickness varying from 2 m at the springings to 1.5 m at the crown (figure 22). Mortar has been interposed only in the first 11 joints at the springings and the 22 joints nearest the crown. The bridge was studied by Castigliano (1879) with the goal of verifying the beneficial effects of mortar joints on the behaviour of the line of thrust. In fact, Castigliano proved that when the mortar is accounted for, the line of thrust is contained entirely within the middle third, while considering the arch ring as a monolith leads to an eccentricity value e at the springing of 0.557 m, as opposed to a middle third value of 0.33 m, corresponding to an opening of 0.682 m at the extrados. In order to obtain this last result, Castigliano considered a linear elastic material and used an iterative procedure.

Our goal is to determine the line of thrust by using the COMES-NOSA code, under assumptions of infinite compressive strength and nil tensile strength. The arch ring is considered to be a monolith subjected to a plane strain; it is discretised into 800 elements with four nodes and four Gauss points, arranged in eight longitudinal lines, each consisting of 100 elements. The amount of loads is equal to that considered by Castigliano in his study, but rather than concentrating the total load in 12 points, we have assigned the weight of the arch ring as a body force and the rest of the load (the permanent load and the overload) has been distributed on the extrados. Figure 23 shows the behaviour of the line of thrust. Once the stress state has been determined through the COMES-NOSA code, we calculate the normal force N and the bending moment M in each normal section of the arch by means of an integration composite trapezoidal open rule using 50 intervals. In order to draw the line of thrust, the eccentricity e i. e. the signed distance of the line of thrust from the mean line of the arch is obtained from the well-known formula $e = M/N$.

The line of thrust is contained entirely within the middle-third except in the region delimited by the springing and the normal section 2.87 m from the springing, that is, the approximate region of the first six voussoirs. In particular, the eccentricity value at the springing is 0.616 m, with a corresponding opening of 0.848 m at the extrados. The horizontal component of thrust at the abutments is 3.963 10^6 N/m; this is 17% higher than Castigliano's result (3.2728 10^6 N/m). The greatest compression stress is obtained at the extrados in the springing and has the value of 7.6 MPa. The region characterised by the opening is illustrated in figure 24, where the isostatic lines are also drawn.

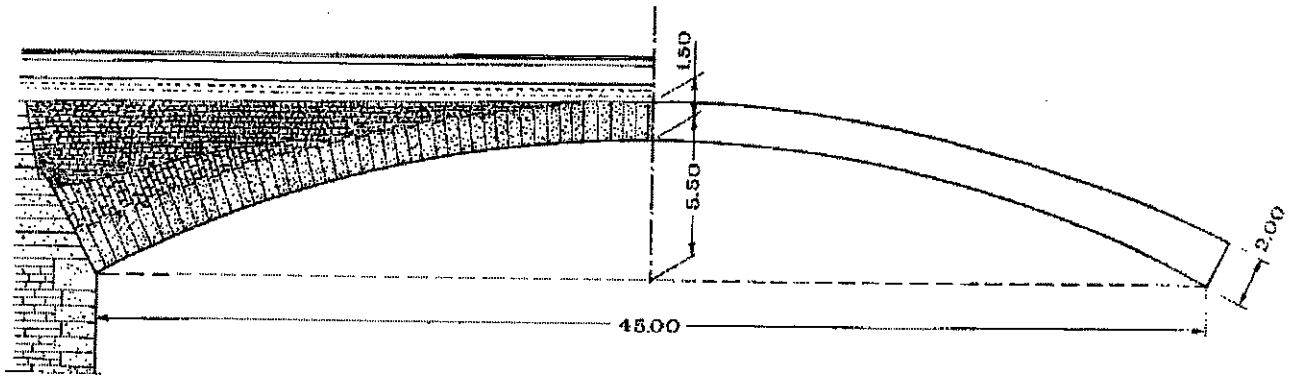

Figure 22. Mosca bridge.

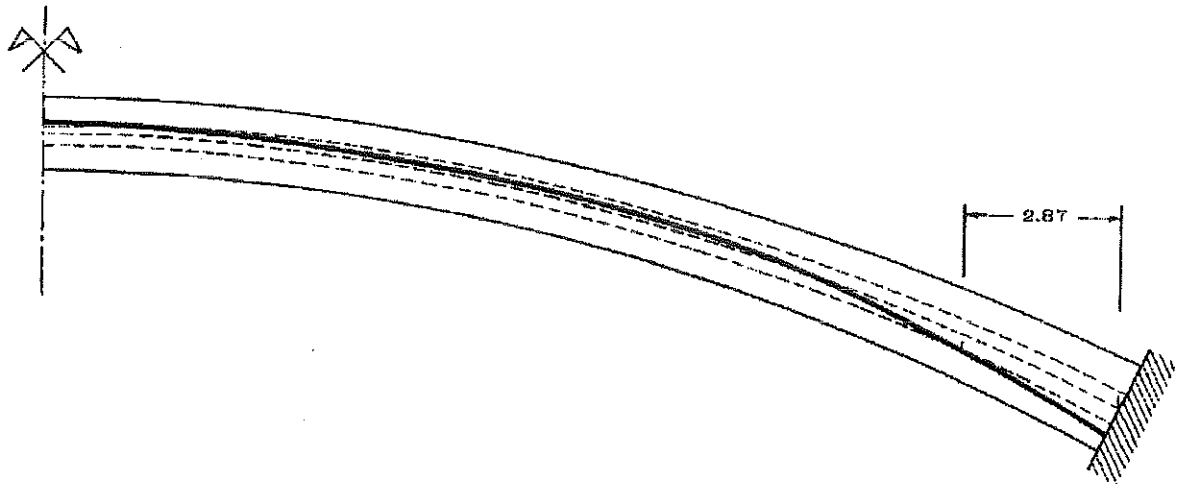

Figure 23. The line of thrust for Mosca bridge.

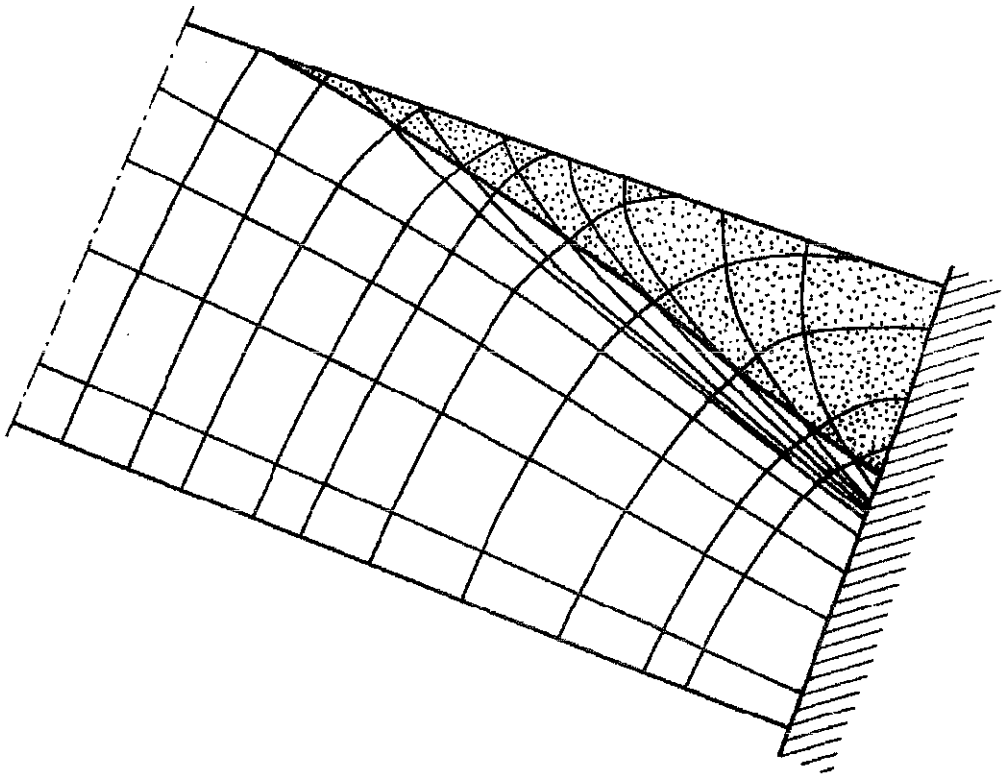

Figure 24. The isostatic lines near the springing.

Bibliography

[1] Castigliano, C. A. P. Théorie de l'equilibre des systèmes élastiques et ses applications. Augusto Federico Negro, Turin (1879).

[2] Lucchesi M., Padovani C., Zani N. "Masonry-like solids with bounded compressive strength". *Int. J. Solids Structures*. 33 (14), pp. 1961-1994, 1996.

The proscenium arch of the Goldoni Theatre in Livorno

The aim of this research was to determine the static conditions of the proscenium arch of the "Goldoni" theatre with the purpose of assessing its safety. To this end, the structure's geometry, loads and state of cracking were analysed, and studies of its masonry and surrounding terrain performed. Then, numerous static analyses of the proscenium arch and its relative piers were carried out. The results, viewed in relation to its current state of cracking, have allowed us to make some hypotheses about the causes of the structure's instability and evaluate the effective safety margin remaining.

Construction of the Goldoni theatre was entrusted to the architect Giuseppe Cappellini (1813-1876) and took four years to complete (1843 to 1847). The building (figure 25) is about 80 meters in length, 40 in width and reaches a maximum height of 25 m. It has a horseshoe-shaped main auditorium. The stage area is separated from the auditorium by a masonry arch, connecting the ends of the "horseshoe" at the gallery level and supported by two box structures, holding the first two rows of loges nearest the stage.

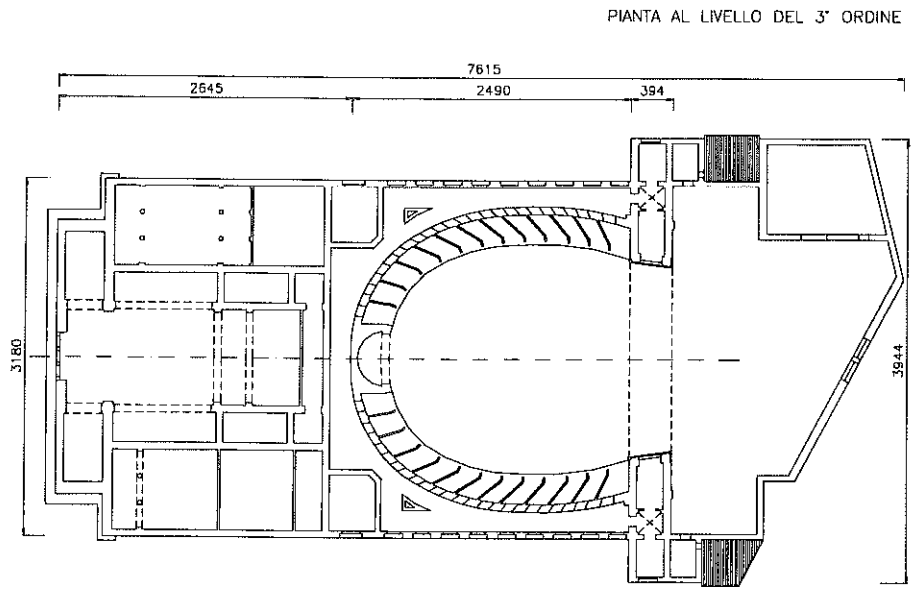

Figure 25. Schematic floor-plan of the theatre at the third tier.

The study performed was prompted by the evident signs of instability in the structure of the proscenium arch. In fact, considerable cracking can be noticed at the level of the arch springings,

especially on the right side (as viewed from the theatre entrance), as well as on the upper part of the supporting pillars, the stage perimeter walls and the inner and outer surfaces of the plastered walls above the arch. The most significant are those that originate at the springings and course vertically upwards to arrive as far as the roof and those present on the walls supported by the arch. Some of these have evidently developed in correspondence to architectural discontinuities, such as niches and discharging arches, but the worst parts seem to involve the arch itself.

The proscenium arch is made up of a cylindrical barrel vault, 3.94 m wide with a net span of 18.7 m, made of brick masonry. It is a raised arch set at the height of 14.7 m from the ground on two box structures housing the vertical rows of theatre boxes flanking the stage.

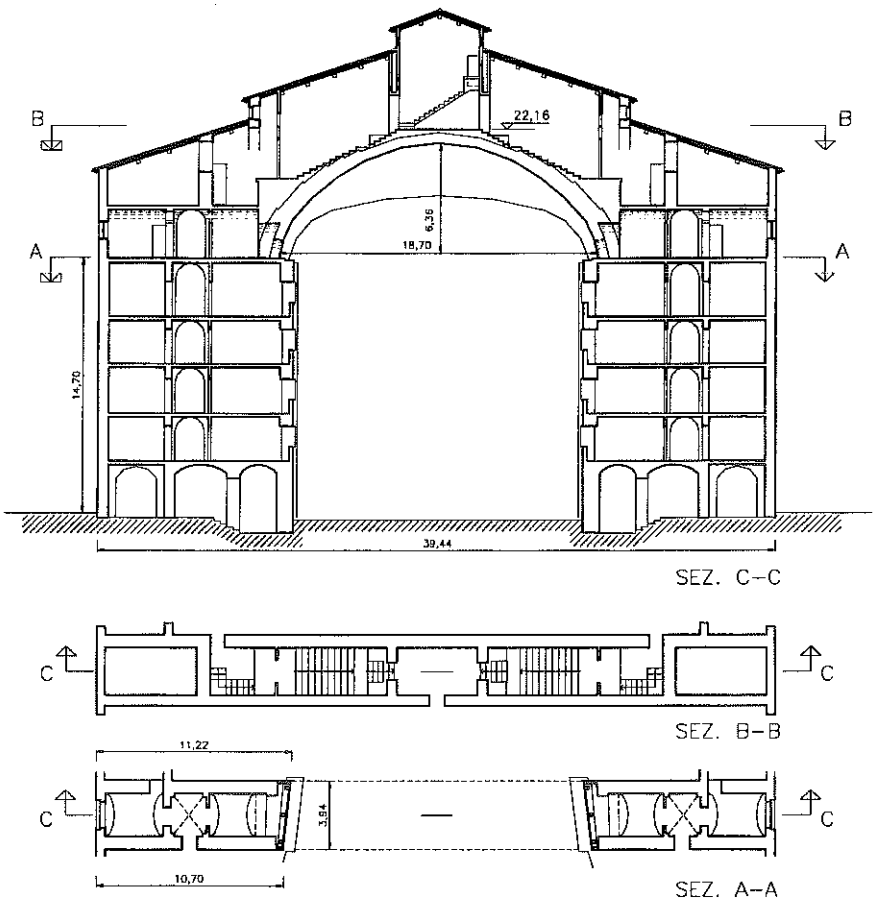

Figure 26. Sections of the structure of the proscenium arch.

The piers, as can be seen in figure 26, are trapezoidal in shape: for geometric reasons, each narrows towards the audience side in order to widen the proscenium opening; the wall on the stage side therefore results to be longer than that on the auditorium side.

Two parallel stone and brick masonry walls (one 60 cm, the other 73 cm) are set lengthwise on the vault to sustain the roof and, therefore represent the virtual continuation of the piers' lateral walls.

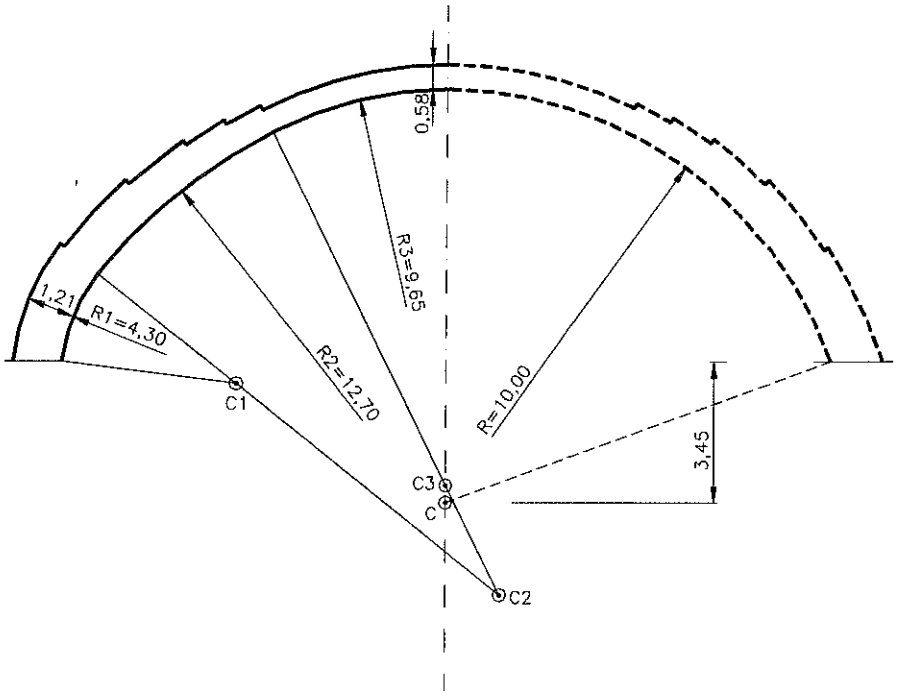

Figure 27. Vault lateral profile.

The intrados shape can be best described as a tricentric curve with radiuses of 4.30 m, 12.70 m and 9.65 m from the springings to the keystone, though it can be approximated quite well by the arc of a circle of radius of about 10 m, whose centre is set 3.45 m below the level of the springings (figure 27). The extrados, as observed from the stage side, runs parallel to this curve but is offset; in fact, the thickness progressively decreases, from a maximum of 121 cm at the springings to a minimum of 58÷60 cm at the keystone.

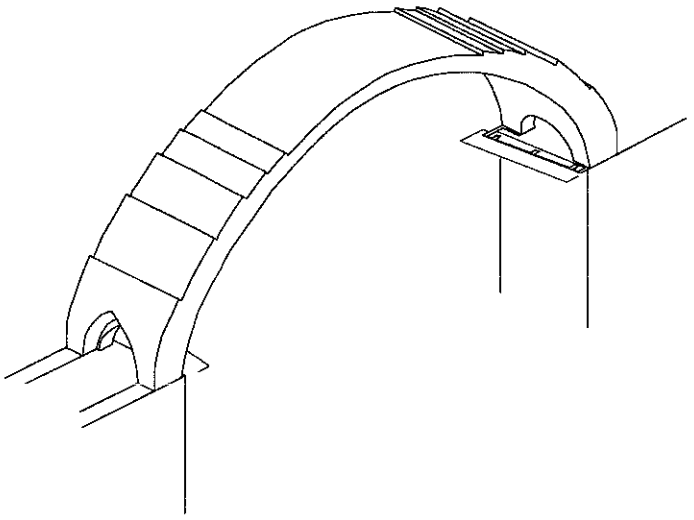

Figure 28. General layout of the arch.

Moreover, the arch does not rest on the springings for its full width, but ends in a small transverse arch, whose span is 2.5 m, that directs the stress flow onto the two longitudinal walls of the piers; an ogival counterarch completes the springings, as shown in figure 28.

For the purposes of its static functioning, the complex structure described in the foregoing can be considered to be symmetrical along the longitudinal plane, and the large vault can be thought of as made up of two parallel load-bearing arches that connect the extremities of the pier walls. The simplified calculation model adopted in this study is based precisely on this consideration.

The structure of the proscenium arch has been studied using different plane and three-dimensional models under different loading conditions. From the geometrical point of view, all are symmetrical. The three-dimensional model has been useful above all because it has provided indications of a qualitative nature that underpin the use of the two plane models. We have limited the study to a plane structure composed of one of these two arches. Specifically, we have chosen the one on the stage side with its corresponding pier walls, because it is the more highly loaded of the two (marked off by the dashed line in figure 29).

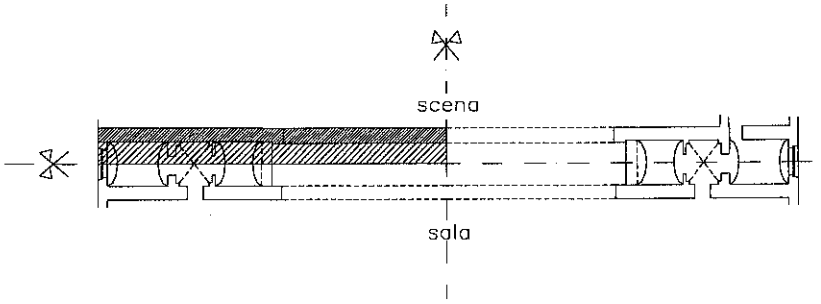

Figure 29. Plan of the proscenium arch (dashed box indicates the modelled part of structure).

The first plane model regards the 0.73 m-thick stage-side arch set on its relative pier wall, which is 0.75 m in thickness. In profile, the arch is can be schematised as the vault shown in figure 30: the pier wall has a height of 14.75 m and width of 10.22 m. The structure is clamped at the base and constrained by symmetry conditions with double pendulums with horizontal-axis at the keystone.

The mesh is made up of 4403 plane 8-node elements, for a total of 27396 degrees of freedom; the analysis has been conducted assuming the structure to be subjected to a state of plane stress.

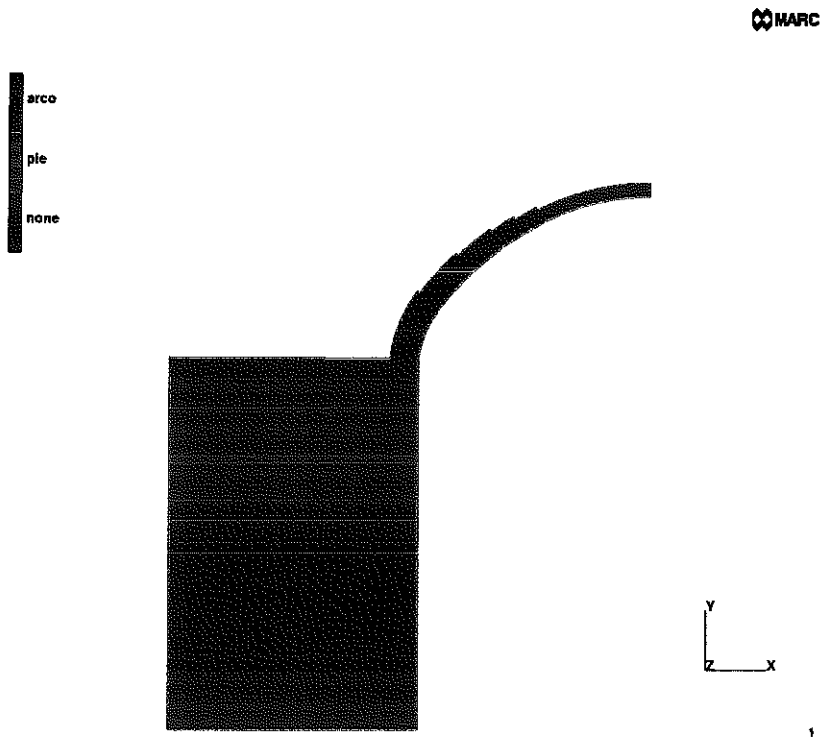

Figure 30. Model 1.

In the second plane model, we also discretise the walls superincumbent on the arch and pier. The thickness of the arch and overlying wall is 0.73 m, while the thickness of the pier and its wall is 0.75 m.

From analysis of the state of cracking of the walls incumbent on the arch (figures 31 and 32), it turns out that the wall portion near the keystone is completely separate from the rest of the structure and acts only as a weight on the vault itself. For this reason, this part of structure has been eliminated from the model and considered as a distributed load on the arch (figure 33). As in

model 1, the structure is fixed at the base and constrained by symmetry conditions at the keystone with double pendulums with horizontal axis.

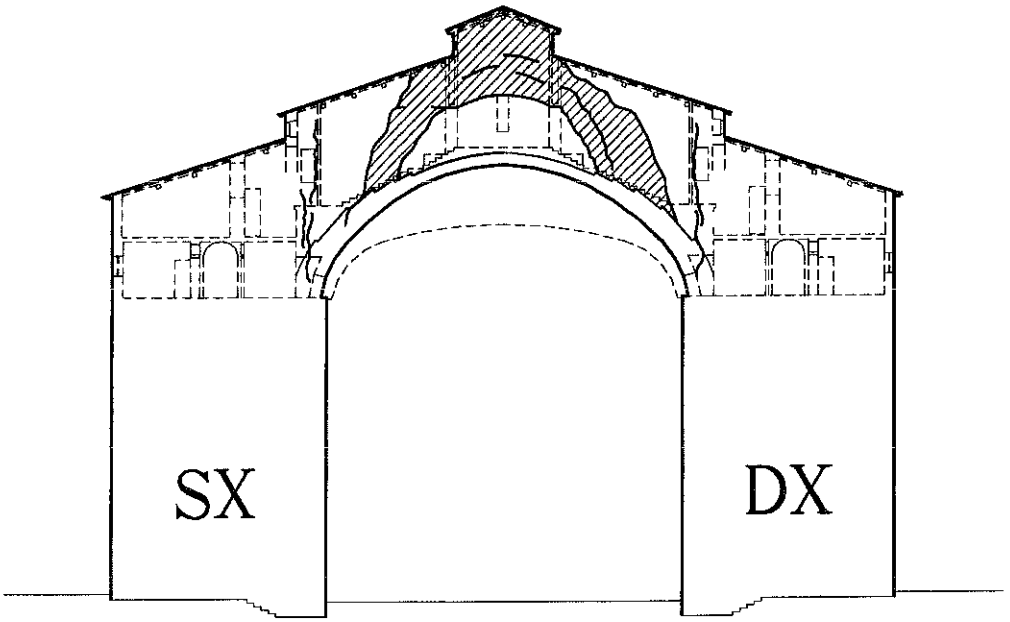

Figure 31. Cracking state, audience side.

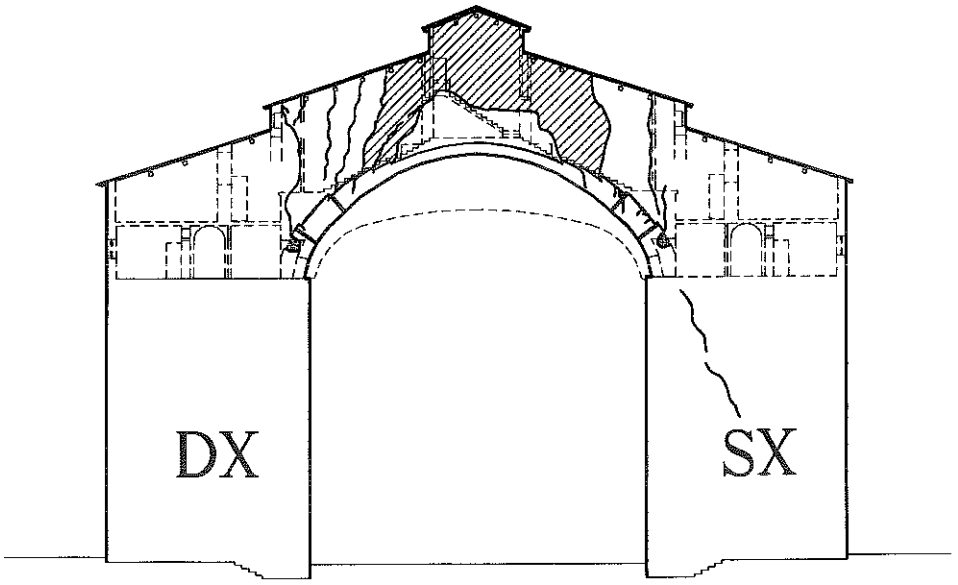

Figure 32. Cracking state, stage side.

The mesh is made up of 6061 plane 8-node elements, for a total of 37096 degrees of freedom; the analysis has been conducted assuming the structure to be subjected to a state of plane stress.

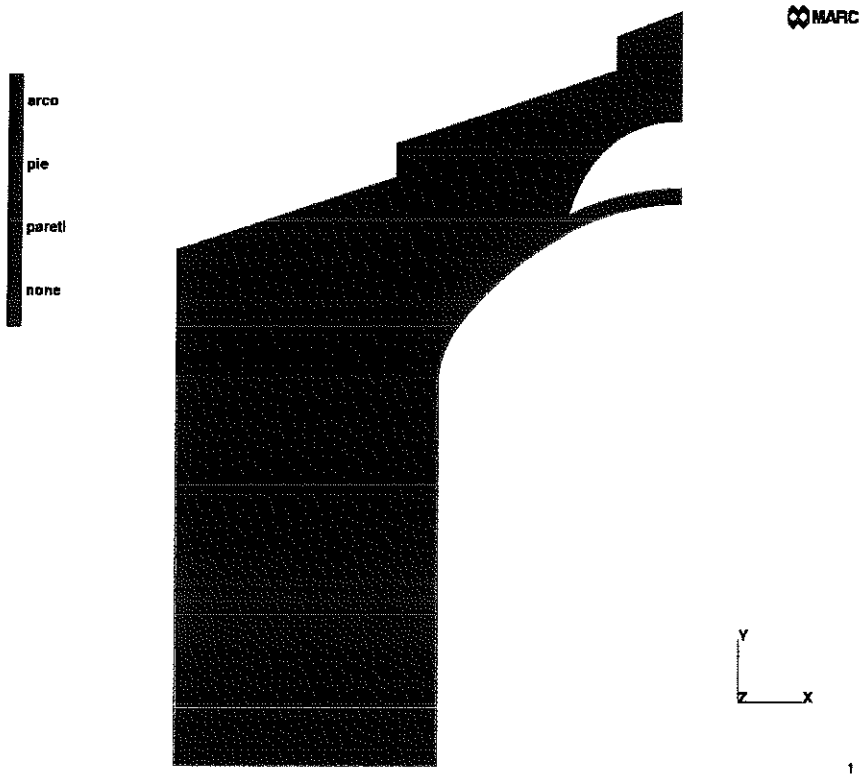

Figure 33. Model 2.

Models 1 and 2 have been used to examine a number of situations by assigning different values of Young's modulus to the various constituent masonries. This was done with the aim of evaluating the strength contribution of the walls overlying the arch, as well as the influence of the pier's deformability. Specifically, the followings four cases have been considered:

	Model	E_{pier} (daN/cm^2)	E_{arch} (daN/cm^2)	E_{wall} (daN/cm^2)
Case I	1	30000	50000	—
Case II	1	15000	50000	—
Case III	2	30000	50000	10000
Case IV	2	30000	50000	1000

where E_{pier}, E_{arch} and E_{wall} indicate the values of Young's modulus used for the masonry constituting the pier, arch and walls overlying both, respectively. In all cases, it is assumed that $\nu = 0.1$.

With the aim of assessing the effects on the structure of eventual subsiding of the terrain, in all cases considered, after conducting the analysis in the sole presence of the loads described above, a vertical displacement δ was applied on the external corner of each pier (figure 34). The displacement is equivalent to an infinitesimal rigid rotation

$$\alpha = \frac{\delta}{L},$$

where L = 10.22 m is the pier's thickness. The vertical displacement δ is applied incrementally in steps of 0.5 cm up to a maximum value that, in light of the ground characteristics, was assumed to be equal to 8 cm.

Although it is realistic to assume that any subsiding of the right and left piers would be unequal, a numerical study (not presented her for brevity's sake) has revealed that such differences do not have any substantial influence on the results of the analysis. We have therefore limited the following description of the results obtained to the case of symmetrical settling of the two piers (figure 34).

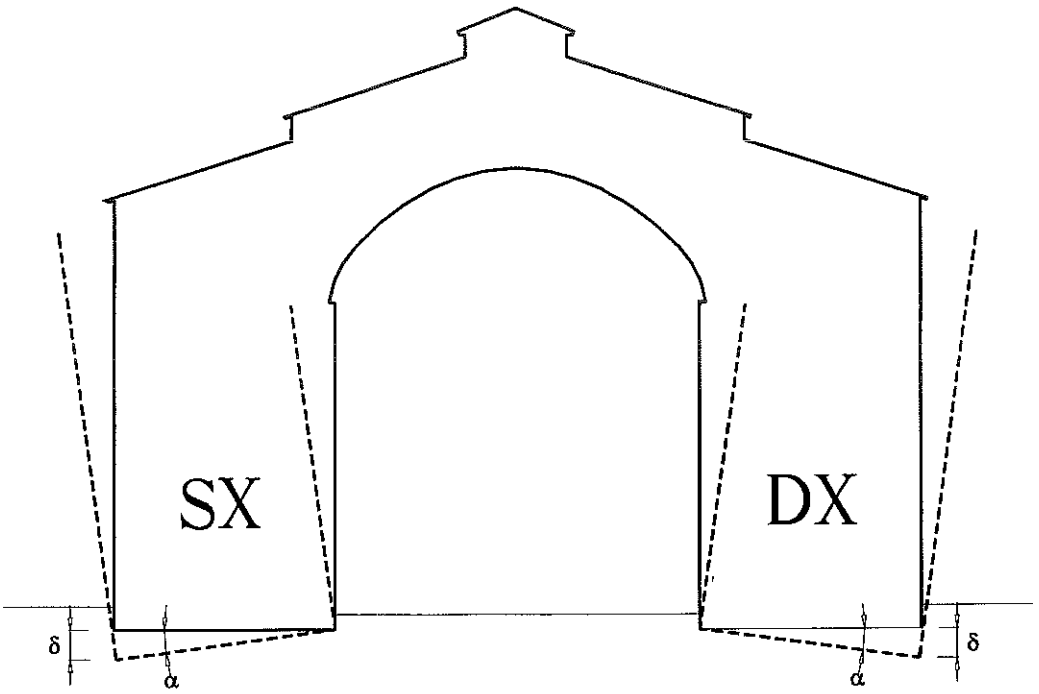

Figure 34. Displacement applied to the piers.

In the following we shall report the results relative to case I alone.

Case I

In this case the strength contribution of the walls superincumbent on the arch and pier is considered nil; the assumed elastic moduli are:

$E_{arch} = 50000$ daN/cm^2	arch masonry Young's modulus,
$E_{pier} = 30000$ daN/cm^2	pier masonry Young's modulus,
$\nu = 0.1$	Poisson's coefficient,

and the load conditions and constraints are the same as in the first model.

The stresses obtained through the finite-element analysis are used to calculate (for the arch alone) the normal strength N, the bending moment M, the shear stress T, the ratio T/N and, through analysis of the combined compressive and bending stresses, the maximum stress σ_M and height a of the non-reacting portion of the section.

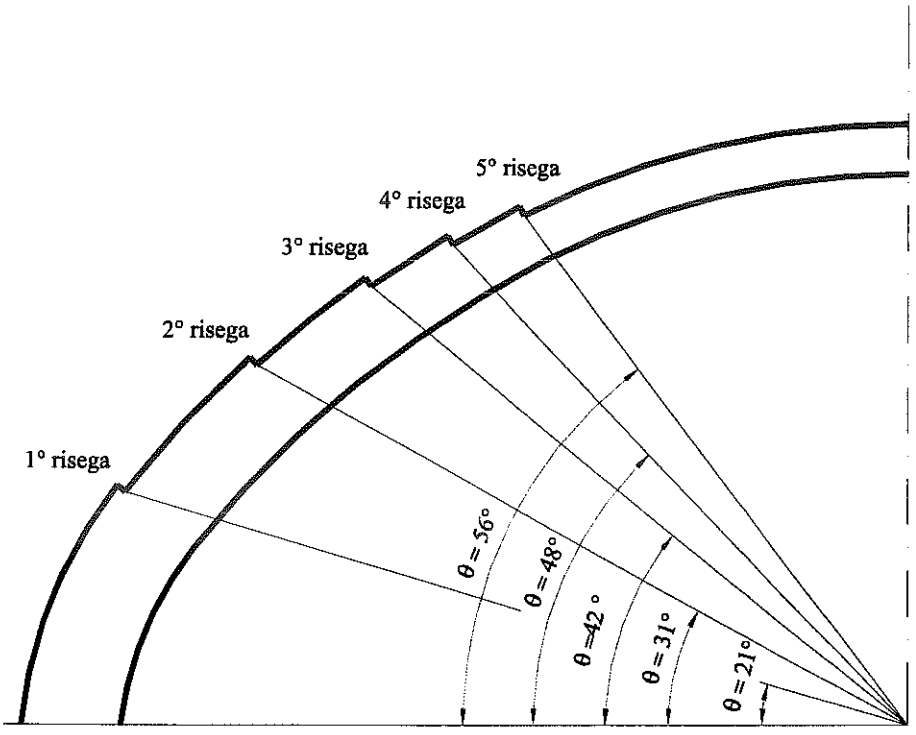

Figure 35. Anomalies at the offsets.

The following figures show the line of thrust in the arch, the isostatic lines and the principal compressive stress pattern in the pier and the arch for $\delta = 0$.

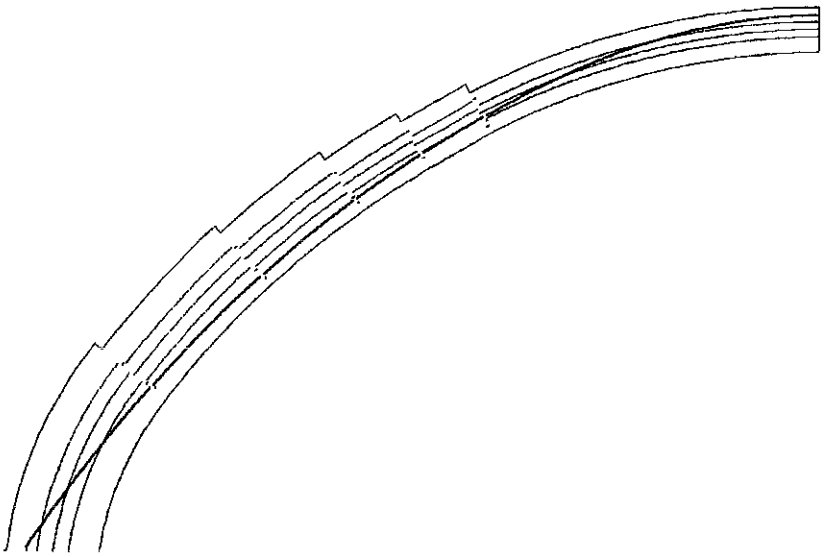

Figure 36. Line of thrust for δ = 0 cm. Case I.

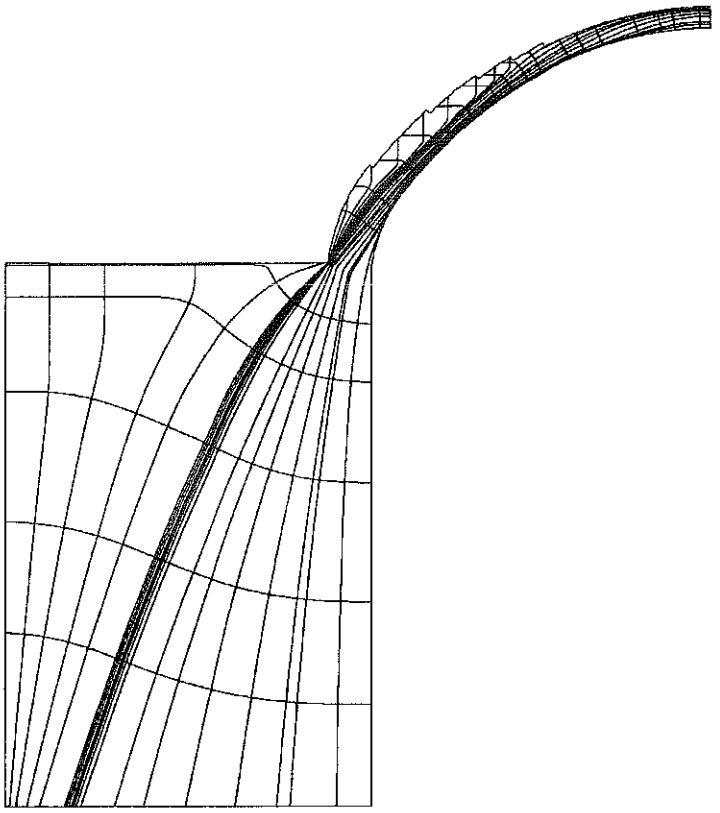

Figure 37. Isostatic lines for δ = 0 cm. Case I.

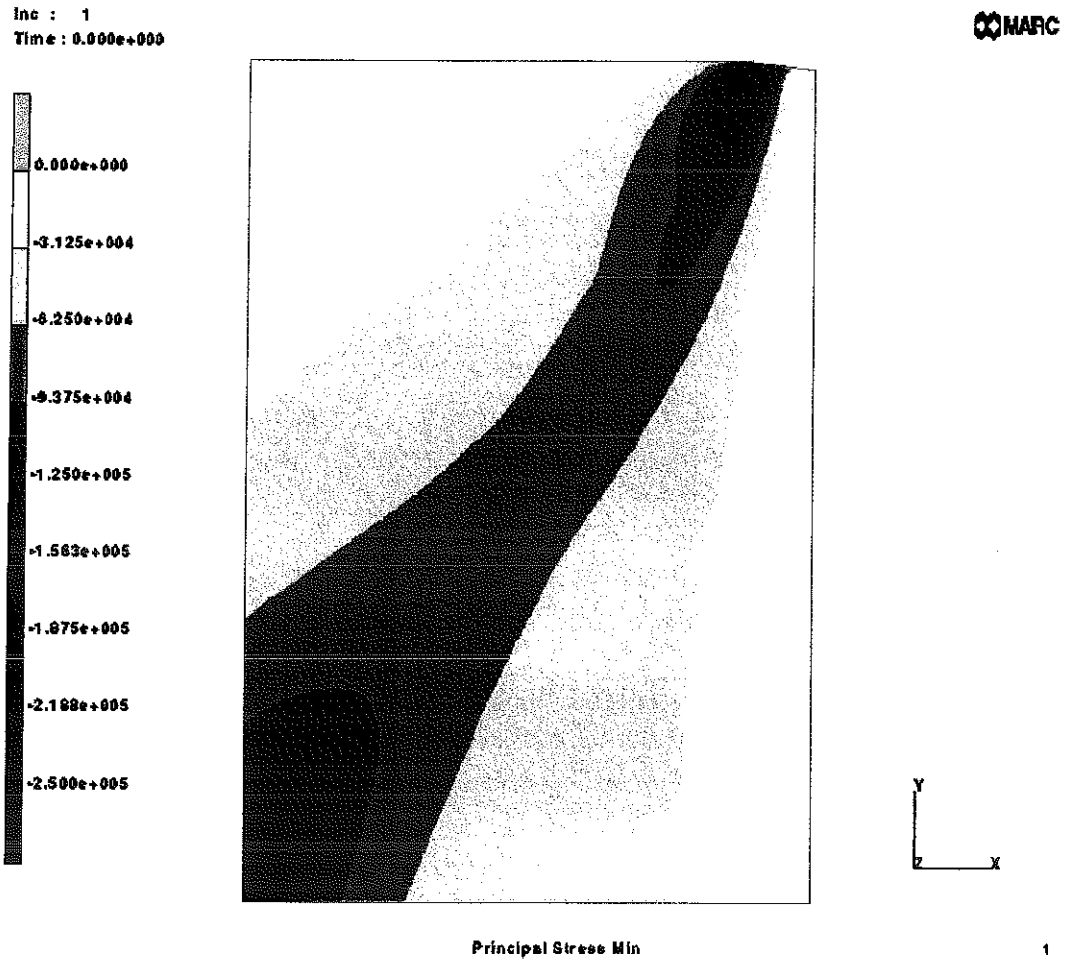

Figure 38. Distribution of the principal compressive stresses (daN/m^2) in the pier for δ = 0. Case I.

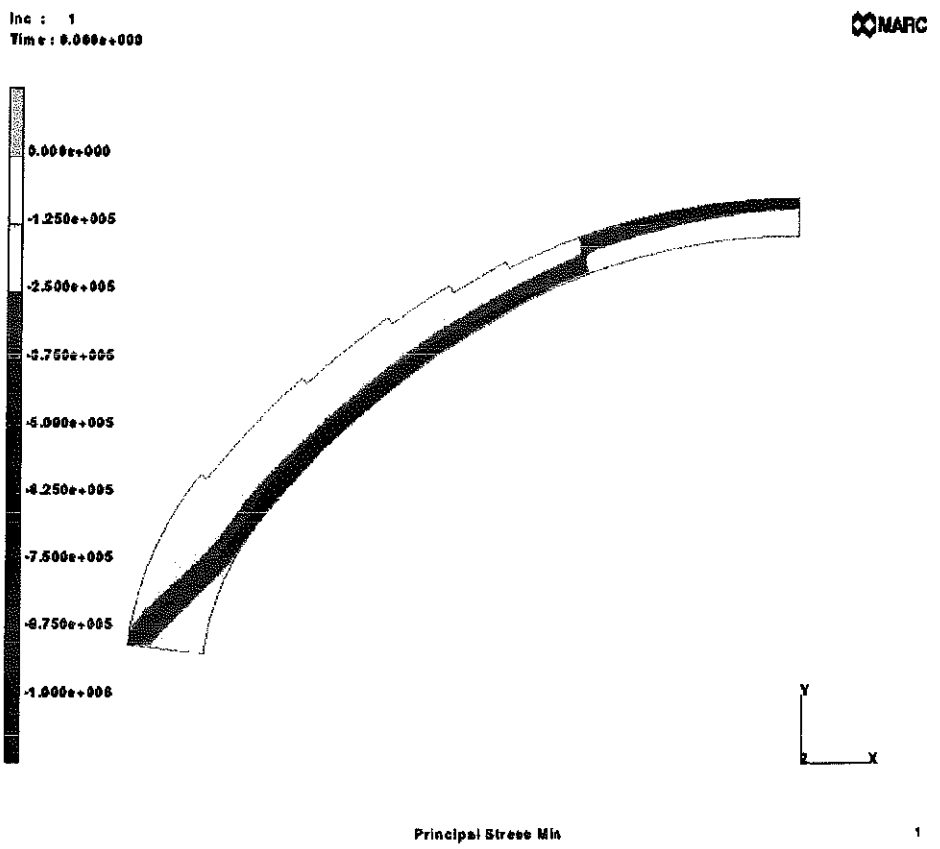

Figure 39. Distribution of the principal compressive stresses (daN/m^2) in the arch for δ = 0 cm. Case I.

It can be observed that neither the normal force N nor the shear force T present appreciable variations, with changing δ. Instead, an increase in the bending moment M is found, especially in correspondence to the first offset, together with the maximum compressive stress σ_M which, for θ = 32.5^O, varies from 71 daN/cm^2 for δ = 0, to 129 daN/cm^2 for δ = 8 cm. An increase in the value of σ_M with increased subsidence is also found at the keystone. It is important to observe that, even in the absence of rotation, when the contribution of the walls overlying the arch and piers is neglected, very high maximum compressive stress results; naturally with increasing δ the situation worsens rapidly.

It should also be noted that T/N, which remains nearly constant with varying δ, equals about 0.5 in the proximity of springing. Such a high value is due to the simplified scheme used in model 1, which neglects the contribution made by the wall overlying the pier to containing the thrust of the arch at the springing. This contribution ranges from 99100 daN for δ = 0 to 94200 daN for δ = 8 cm.

Finally, in the proximity of the second offset, the height of the resistant section of the arch diminishes from 54 cm for $\delta = 0$, to 29 cm for $\delta = 8$ cm. In effect, as can be gathered by observing the state of cracking a large part of the arch's section turns out to be non-operational in correspondence to the haunches.

Bibliography

[1] Lucchesi M., Padovani C., Rini C., Sassu M., Zani N. "Experimental tests and numerical modelling for the scenic masonry arch of the historic *Teatro Goldoni* in Livorno". *Fourth International Masonry Conference*, Cumberland Hotel, Marble Arch, London 23-25 October 1995.

[2] Lucchesi M., De Falco A., Zani N. Studio del comportamento statico dell'arco scenico del treatro Goldoni di Livorno. Relazione Tecnica (1998).

The Medici arsenal in Pisa

At request of the University of Pisa, a study was conducted of the Medici arsenal using the COMES-NOSA code. The aim of the study was to model some restorative operations to improve the structure's seismic resistance, evaluate their effectiveness and allow making the best choices in order to guarantee the safety and functionality of the building, which is destined to house university classrooms in the future.

In the 16th Century the de'Medici assigned the role of second city of the new "State" to Pisa by virtue of its age-old and illustrious history as a maritime republic and its strategic position on the Tyrrhenian sea. The city had a centuries-old tradition of ship-building. The north-west bank of the Arno river and a vast area surrounding it had been given over to this enterprise when it was decided to fortify the zone by constructing a true citadel to defend against access from along the river on the city's western end. Within the citadel's interior was housed "the republican arsenal", a structure originally used as a factory, nearly entirely buried now, constructed in the forms and materials typical of medieval Pisan architecture. This building and its relative dock were deemed unsuitable to satisfying the plans to create a great new fleet, so it was decided to establish the new arsenal here. The choice of the location fell on the area overlooking the Arno running approximately from the entrance to the bridge of the Citadel to the churches of Sant'Agnese and San Vito, which was taken up partly by the monastery of the former church and given over to Gardens (*il Giardino dei Semplici).*

The building, which was arranged in eight aisles (figure 40), had a simple enough structure: pillared arches, saddle roof with wooden counterlath set on purlins and rafters and roof covering in keeping with traditional Tuscan architecture. The arches were devoid of chains so as not to obstruct construction of the galleys above; the thrust of the transverse arches was supported on one side by the aisle abutting on the church of San Vito and on the other, by a small additional aisle set scarp buttres fashion. As has also been corroborated by essays from the time, the inside arcades were completely free, without that fire-stop walls that Alberti suggested were present, just as the overlooking arcades were also open to the river. The contribution of Bernardo Buontalenti to this shipyard has been attested to: Baldinucci reports that the renowned architect provided "planning and assistance", and perhaps also the design of the beautiful Medici coat of arms with the the still visible cardinal's insignia of Ferdinando set on a sail in the center of the façade bearing the date 1588.

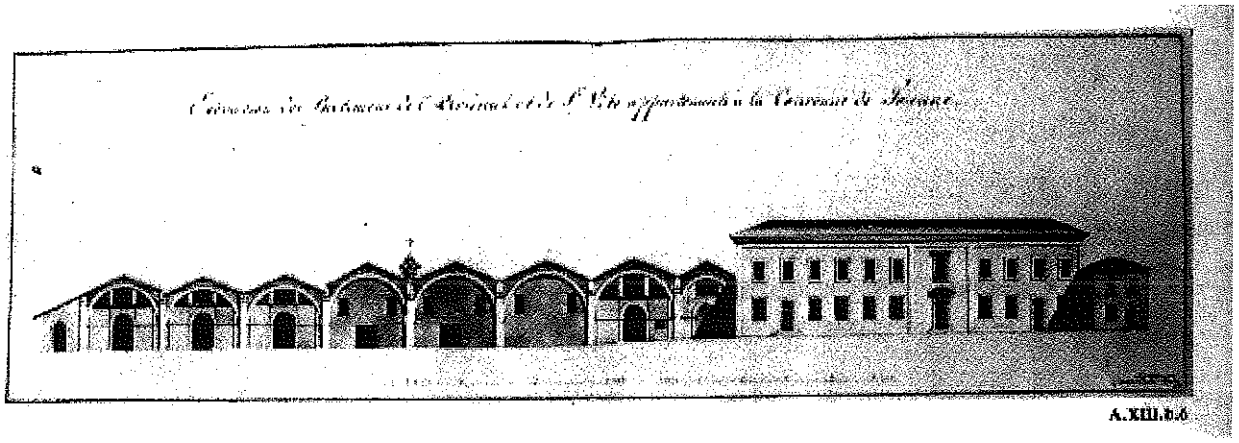

Figure 40. View of the Medici arsenal overlooking the Arno.

After the complex had outlived its usefulness as an armory, it suffered many losses and underwent many modifications. In the late 18th Century external buffering of the arches was performed and the floor level was raised with a stone pavement in order to create horse stalls. On this occasion seven bays adjacent to San Vito were demolished to create a new courtyard, and the roofs of the last three aisles to the west raised to bring them to the same height as the others, thereby increasing the walls above extrados of the arches. Still more serious damage was inflicted during the last war, with loss of the western aisle, including the section flanking it.

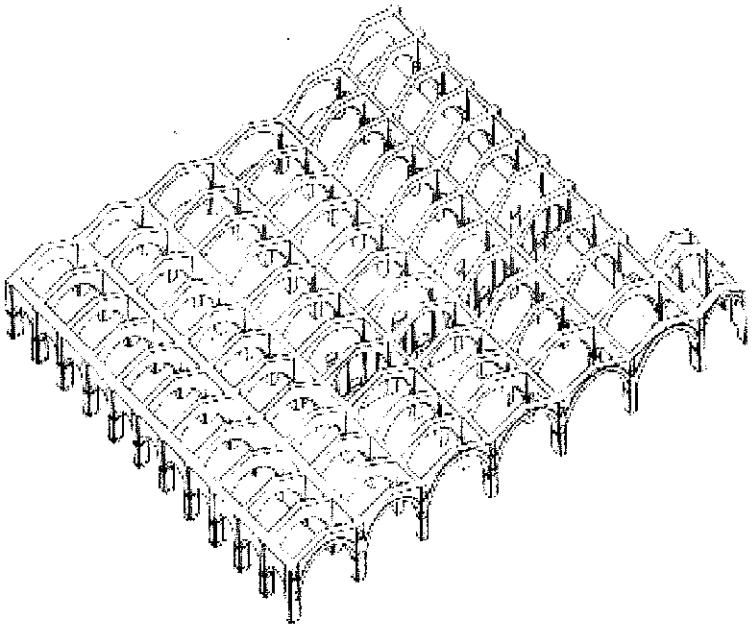

Figure 41. Series of arches making up the current structure of the arsenal.

The structure, whose architectural merits appear evident even today, is made up of a set of pillars surmounted by full ogival arches (figure 41). The series of parallel arches on the building's main façade (W-E direction) have an average height at the keystone of about 8.7 m, while those laid parallel to the aisles' axes have a height of about 4.7 m; from the third aisle onward, these are for the most part closed in by masonry walls. The one exception to this is along the direction of the "roadway" that crosses the entire arsenal from west to east. In this direction, the series of arches in the first four aisles (beginning from the west) form an angle of 15° with those in the N-S direction. The arches of the fifth and the sixth aisles, on the other hand, are orthogonal to each other; this is owing to the fact that each series of arches arranged in the W-E is rotated counterclockwise by 15° in correspondence to the fifth pillar.

Currently the structure is devoid of any sort of buttress able to sustain the thrust of the arches. On the building's western side, an attempt was made to compensate, at least partially, for this situation by chaining the arches of the last aisle. Recently, restoration work has been initiated by the Soprintendenza per i Beni Ambientali Architettonici Artistici e Storici of Pisa and, as part of the re-roofing operations, the filling material has been substituted with reinforced concrete beams above each series of arches along both the W-E and N-S directions. Such reinforced concrete beams remain to be inserted on all the arches of the western aisle and on nine arches of the eastern aisle.

The effects of seismic actions directed parallel to the building's main façade have been determined (earlier studies had in fact revealed that there are no static problems with regard to actions parallel to the aisles' axes.) To this end, the structure has been analyzed, in its current state, as well as with retaining structures applied to the E and W sides of the building and with the application of both retaining structures and chains. The action of an earthquake is simulated by a horizontal body force, constant throughout the structure's height. Since, given its dimensions, it is impossible to arrive at a finite-element model of the whole structure, it was decided to analyze that part, made up of three series of arches, situated immediately to the north of the roadway. This part of the building was measured and subjected to experimental materials tests.

The finite-element code COMES-NOSA has been applied to analyzing the structural behavior of the building subjected to its own weight, the weight of the roofing and a horizontal load parallel to the building's main façade. In order to discretize the structure, a non-conforming shell element with eight nodes was used, based on the Kirchhoff-Love hypothesis.

The reinforced concrete beams, as well as the steel beams making up the retaining structures and chains have been assumed to be linear elastic. The masonry, on the other hand, has been

considered an elastic material not withstanding tension, for which the following parameter values, deduced through laboratory tests performed at the University of Florence Constructions Department on materials sampled on the arsenal, have been used:

Young's modulus of the masonry	$E_m = 4.5\ 10^4$ daN/cm^2,
Poisson's ratio of the masonry	$\nu_m = 0.12$,
Ultimate compressive stress of the masonry	$\sigma_{mr} = 100$ daN/cm^2.

The structure has been studied under three different conditions:

(a) in the presence of retaining structures applied to the eastern and western sides of the building,

(b) in the presence of retaining structures as in point (a), together with chains fitted in the W-E direction and connected to the retaining structures and pillars,

(c) in the structure's actual state, neglecting the existing chains on the western aisle.

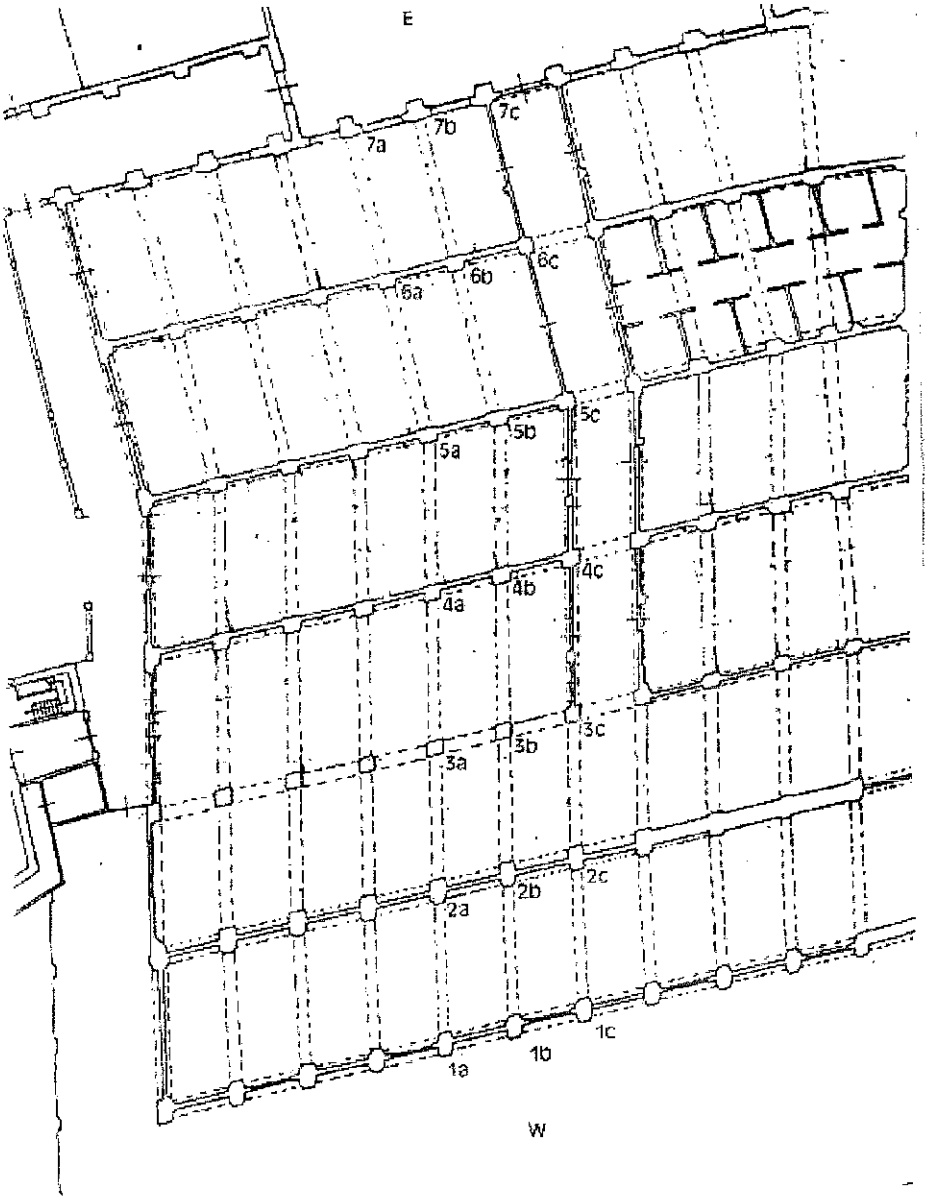

Figure 42. The two rows of pillars 1a-7a and 1c-7c delimiting the portion of the building analyzed with the COMES-NOSA code.

The part of structure considered first is made up of three series of arches parallel to the building's main façade, indicated in figure 42 by the rows of pillars 1a-7a and 1c-7c. Metal retaining structures were fitted to each series of arches. As this was a preliminary study, accurate planning

of these structures was not performed; each has been schematized as made up of two beams and a plate adhering perfectly to the pillar and overlying filling material.

Overall, 25185 elements were used, for an approximate total of 150000 degrees of freedom. The dimensions of the mesh needed to discretize the three series of arches render the calculations extremely onerous. Therefore, in order to study cases (b) and (c), a simpler structure has been considered, that is, one made up of a single series of arches to which some elastic side supports were added, one for each pillar, to simulate the action of the masonry walls. The analysis in point (a) was repeated by applying the model to three series of arches, and the good agreement between the results obtained using the two different models bears out the validity of employing the simplified model in cases (b) and (c).

In all the cases considered the bases of the pillars are clamped. In case (b) the chains, set at a height of 4.16 m from ground level, have an extensional stiffness of 1.89 10^7 daN and are connected to both the retaining structures as well as the individual pillars, to which they are connected by steel plates. The chains have been assumed to have a pretension level of about 2000 daN.

The structure's own weight is applied as a vertical body force calculated on the basis of each material's corresponding specific weight (1800 daN/m^3 for the masonry, 2500 daN/m^3 for the reinforced concrete and 7800 daN/m^3 for the steel). The overall weight of the roofing is assumed to be 180 daN/m^2 and is applied to the structure by opportunely increasing the specific weight of the reinforced concrete beams set in the W-E direction.

The horizontal load, which simulates the action of an earthquake, is assigned as a body force and, given the structure's modest dimensions, is assumed constant throughout its height In each case, the loads have been assigned incrementally. The vertical loads are applied at the first increment, while the horizontal loads are assigned over the subsequent increments by progressively increasing the ratio C between horizontal and vertical loads up to 0.28, with a step of 0.035 for each increment.

The numerical results obtained using the COMES-NOSA program have been analyzed according to the following scheme. Firstly, we consider case (a), studied using the three-arch-series model, and subsequently, take up cases (b) and (c) performed through the simplified model. For each case and every load increment we determine:

1. the reacting section at the base of each pillar, the maximum compressive stress attained and the mean shear stress;

2. the significant internal forces on the reinforced concrete beams set in the W-E direction, in order to determine the stresses in the chains and concrete.

Moreover, for case (a) we have studied the behavior of the arches in the W-E direction, as well as that of the masonry walls, the reinforced concrete beams in the N-S direction and the retaining structures. Subsequently, we determine the excess probabilities of some quantities deemed particularly important to assessing the building's safety.

Case (a)

From the stresses obtained for each pillar with the finite-element analysis we have calculated the normal force N, the bending moment M_1 acting on the mean plane of the pillar, the bending moment M_2 perpendicular to M_1 and the shear force T_1 parallel to the mean plane. At the base of the pillars considered the maximum compressive stress sgm has been calculated, with an analysis of the combined compressive and bending stress, and the mean shear stress tgm on the reacting section. The greatest values of sgm are found at the base of pillars 5 and 6. This is owing to the fact that the stress center at the base of these pillars is also eccentric in the direction orthogonal to the mean plane because of the 15° rotation of the last two arches with respect to the preceding ones.

The highest shera stress values are found at the base of pillar 5. With regard to the reinforced concrete beams, no significant differences have been found between the results from beams belonging to different rows of arches. The most highly stressed chains are the upper ones on beam 1 and the maximum tensile stress sgt1 reaches the admissible stress value σ_{af} = 2200 daN/cm^2 at C = 0.13 and the yield value σ_{sf} = 4400 daN/cm^2 at C = 0.22.

Case (b)

Also in this case (structure fitted with both retaining structures and chains, analyzed with the simplified model) the most elevated values of sgm are found at the base of pillars 5 and 6.

As in the preceding case, the most stressed chains are those on the first beam. For C = 0.21, the results do not differ significantly from those obtained in case (a), while for C = 0.28, the maximum value of sgt1 was found to be lower by about 18%. The maximum tensile force in the chains for C = 0.28 results to be about 3500 daN.

Case (c)

In this case (structure in its actual state, though devoid of the chains on the western aisle, analyzed with the simplified model composed of a series of arches with no retaining structures), the horizontal load has been applied only for C = 0.21. The absence of the retaining structures also allows analyzing the data relative to pillars 1 and 7. The highest values of the maximum compressive stress sgm are at the base of pillars 5, 6 and 7; at the base of pillar 7, this reaches the value of 93 daN/cm^2 at C = 0.21. In this case the most highly stressed reinforced concrete beam is the fifth one.

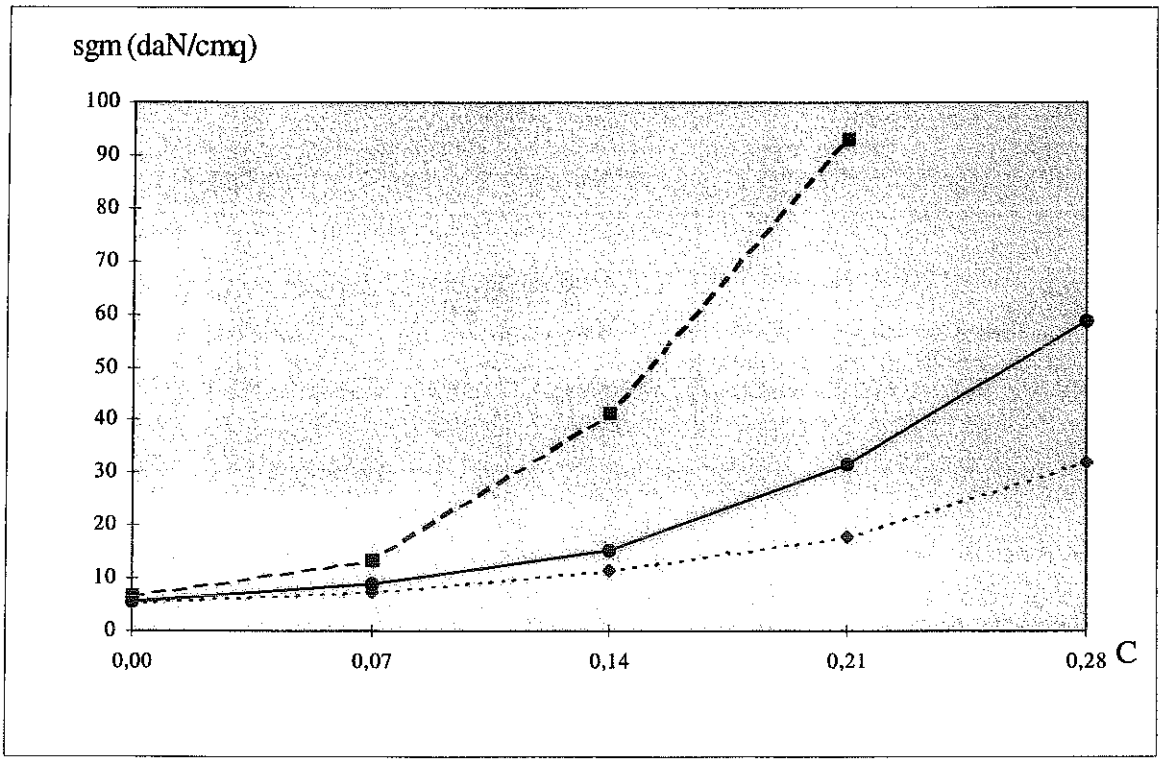

Figure 43. Comparison of the sgm pattern as a function of C, in cases (a), (b) and (c).

Figure 43 presents a comparison of the values of sgm obtained in cases (a) (continuous line), (b) (dotted line) and (c) (dashed line). The data is relative to pillar 5 in cases (a) and (b) and pillar 7 in the case of (c).

The data relating to the seismic risk in Pisa have been drawn from the catalogue compiled by the National Group for Earthquake Defense of the C.N.R and developed within the framework of the collaboration agreement between the Research Institute on Earthquake Hazard of the C.N.R and the Tuscan regional Department of the Environment.

The graph in figure 44 allows determining the probability that an earthquake with ground acceleration equal to or greater than γg occur in the intervals of time ΔT = 50 years (continuous

line), 100 years (dotted line) and 500 years (dashed line) for each value of γ (ratio between ground acceleration and that of gravity, g = 10 m/sec^2).

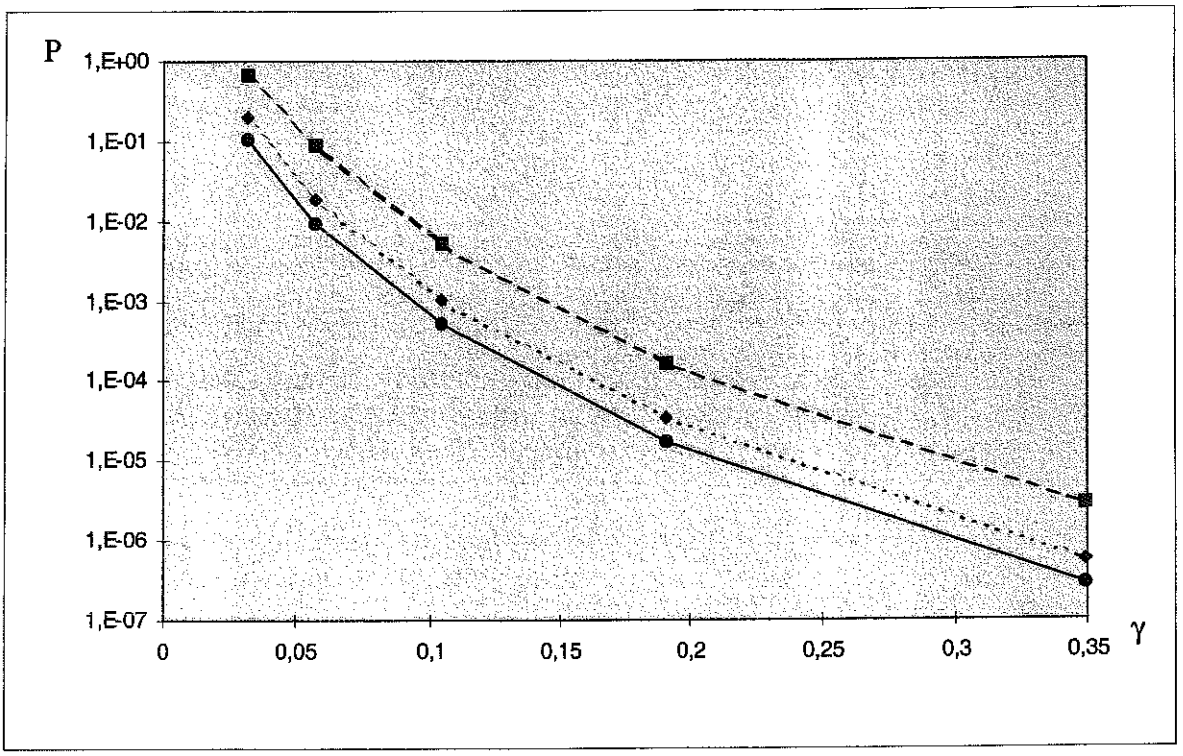

Figure 44. Probability that an earthquake occur with ground acceleration equal to or exceeding γ g, for Δ T = 50 years (continuous line), 100 years (dotted curve) and 500 years (dashed curve). Ordinates are in logarithmic scale.

Given the modest height of the building, it appears reasonable to assume that the horizontal acceleration at each elevation does not exceed twice that at the ground. We may therefore set C = 2γ. For each value C_0 of C and for each time interval ΔT, let us indicate by $P_{\Delta T}(C \geq C_0)$ the corresponding probability of exceeding such value. In other words, $P_{\Delta T}$ $(C \geq C_0)$ is the probability that in a period of ΔT years, the ratio between the horizontal and vertical loads acting on the building is equal to or greater than C_0. Knowing the value of $P_{\Delta T}$ $(C \geq C_0)$ with varying C_0 and from the results of the numerical analyses, it is easy to deduce the excess probabilities sgm, tgm, sgt1, etc, for an interval of ΔT years. Figure 45 plots the curve of $P_{100}(sgm \geq sgm_0)$ (the excess probability of sgm_0 (daN/cm^2) for a 100-year period) with varying sgm_0, for cases (a) (continuous line), (b) (dotted line) and (c) (dashed line).

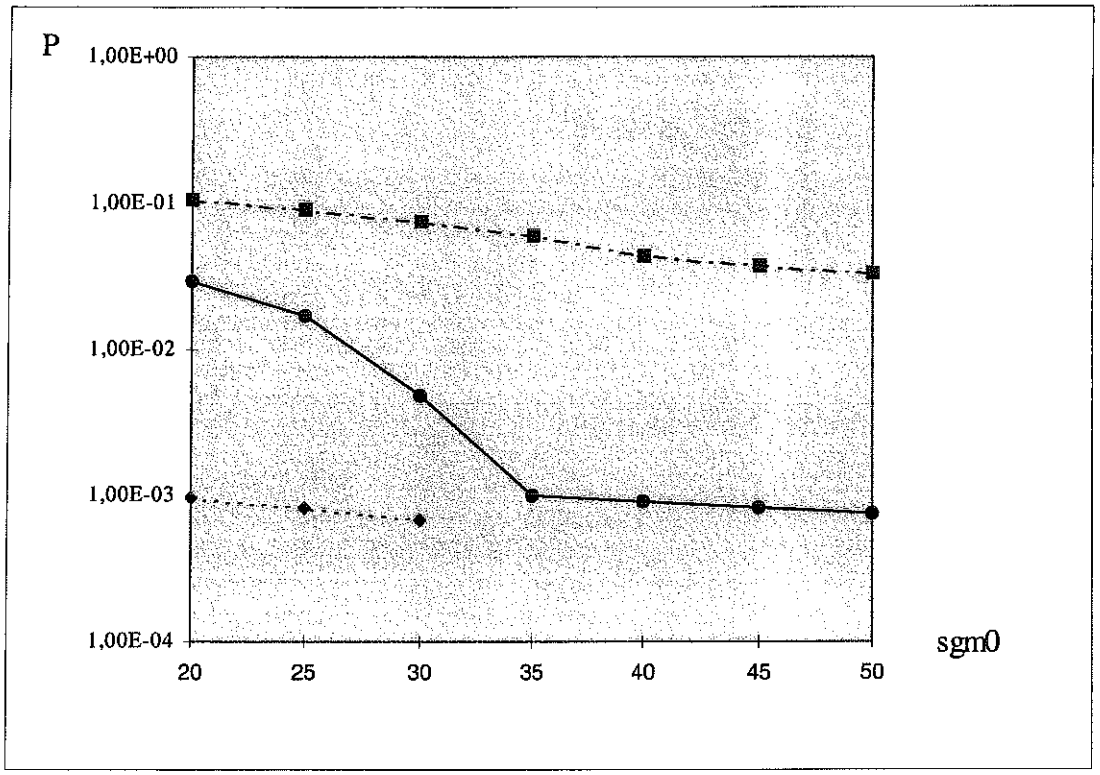

Figure 45. Comparison of the behavior of $P_{100}(sgm \geq sgm_0)$ as a function of sgm_0 in cases (a), (b) and (c). The ordinates are in logarithmic scale.

Regarding the reinforced concrete beams, the probability of exceeding the admissible, yield and ultimate stresses in the chains over a 500-year period are respectively 15%, 5 ‰ and 4.2 ‰ for case (a), 20%, 5 ‰ and 3.25 ‰ for case (b), and finally 42%, 9.6% and 4.9% for case (c).

The analyses performed have underscored the need to carry out consolidation and seismic modifications on the building. It is in fact sufficient to observe that, in its current state, there is a 3.3% probability that within 100 years an earthquake will occur whose intensity is high enough to determine a compressive stress level twice that of the ultimate stress at the base of some of its pillars. Moreover, by simulating two different types of reinforcement measures we have been able to evaluate the improvement that each would bring about in the building's response to seismic loads. In fact, from the results it appeared necessary, at the least, to proceed with the fitting of retaining structures on both the western and eastern sides of the building, bearing in mind, the fact that it is currently lacking any buttress whatever able to sustain the thrust of the arches. This

consolidation work has reduced the maximum stress at the base of pillar 5 by 53 daN/cm^2 for C = 0.21 and cuts down the probability of exceeding half the ultimate stress in 100 years to 8 x 10^{-4}.
A further significant finding is that, although chaining the arches can provide significant further improvements in terms of increased stability, the effect, as can be concluded from figures 44 and 45, is decidedly inferior to that obtained by the retaining structures alone.

Bibliography

[1] Lucchesi M., Zani N., "Analisi sismica di tipo statico dell'Arsenale Mediceo situato in Pisa, lungarno Simonelli" Consorzio Pisa Ricerche, relazione tecnica (1996).
[2] Cecati F., Lucchesi M., Padovani C., Pagni A., Zani N. "Consolidamento e adeguamento antisismico: un modello di calcolo per orientare il progetto". XIV Convegno Scienza e Beni Culturali, Bressanone, 30 giugni-3 luglio, 1998.

No-tension materials in the presence of thermal expansion

In many applications it is necessary to model the behaviour of solids not withstanding tension in the presence of thermal dilatation. For example, molten metal production processes, in particular integrated steel manufacturing, require refractory linings able to withstand the thermo-mechanical actions produced by high-temperature fluids.

However, there are many other engineering problems involving no-tension solids in which thermal dilatation must be accounted for: consider, for example geological problems connected with the presence of a volcanic caldera, such a that of Pozzuoli, or the influence of thermal variations on stress fields in masonry bridges. In many such cases the thermal variation is so high that the dependence of the material parameters on temperature cannot be ignored.

Firstly, we have studied a constitutive equation for isotropic no-tension materials in the presence of thermal expansion that accounts for the temperature-dependence of the material's parameters. This constitutive equation can model the behaviour of a number of refractory materials. In particular, we assume that the thermal expansion is a spherical tensor depending on temperature, $\beta(\theta)\mathbf{I}$, that the total strain minus the thermal expansion is the sum of an elastic part on which the stress, negative semi-definite, depends linearly and isotropically, and a positive semi-definite inelastic part orthogonal to the stress. We thereby obtain a non-linear elastic material conforming to a masonry-like material in the absence of any temperature change.

Subsequently, we have studied numerical techniques for the solution of the equilibrium problem of no-tension solids in the presence of thermal expansion, and these have been implemented in the COMES-NOSA. The code has then been applied to the study of a spherical container subjected to two uniform radial pressure acting on the inner and outer boundary and a steady temperature distribution – a problem for which the solution has been explicitly calculated. Lastly, a masonry arch subjected to temperature change and a converter used in the steel and iron industry have been examined.

Spherical container subjected to two uniform radial pressures and a steady temperature distribution

A spherical container of inner radius a and outer radius b is subjected to two uniform radial pressures p_1 and p_2 acting respectively on the inner and outer boundary, and to a steady temperature distribution θ that varies with the radius r,

$$\theta(r) = \frac{ab(\vartheta_1 - \vartheta_2)}{b-a}\,\frac{1}{r} + \frac{b\vartheta_2 - a\vartheta_1}{b-a} + \theta_0\,, \tag{6}$$

where θ_0 is the reference temperature, ϑ_1 e ϑ_2, with $\vartheta_1 > \vartheta_2$ are defined by $\vartheta_1 = \theta_1 - \theta_0$ and $\vartheta_2 = \theta_2 - \theta_0$, with $\theta_1 = \theta(a)$ and $\theta_2 = \theta(b)$, respectively. We assume that the thermal expansion coefficient β is

$$\beta(\theta) = \alpha(\theta - \theta_0)\,, \tag{7}$$

with α constant; Poisson's ratio is zero and finally, Young's modulus is a decreasing function of temperature

$$E(\theta) = \omega\,\frac{\dfrac{ab(\vartheta_1 - \vartheta_2)}{b-a}}{\theta - \dfrac{b\vartheta_2 - a\vartheta_1}{b-a} - \theta_0}\,, \tag{22}$$

where $\omega = \dfrac{E_1}{a}$ is a positive constant. By virtue of (6) we have

$$\hat{E}(r) = E(\theta(r)) = \omega r\,, \tag{8}$$

in particular $\hat{E}(a) = E_1$, $\hat{E}(b) = \dfrac{b}{a}E_1 > E_1$.

It is possible to arrive at the solution to the equilibrium problem, specifically, the stress state, displacement and inelastic strain.

With the aim of comparing the explicit solution with that calculated using the COMES-NOSA program, half the container has been examined by discretizing it with 800 axisymmetric elements with 8 nodes and 9 Gauss points. In Figure 46, 47, 48 and 49 the explicitly calculated stress components, radial displacement and tengential inelastic strain are represented by the continuous line, while the corresponding quantities determined numerically at the Gauss points are indicated by the asteriks. The graphs have been obtained by using the following parameter values

$a = 1$ m,

$b = 2$ m,

$\nu = 0$,

$E_1 = 2.5\ 10^9$ Pa,

$\alpha = 1.\ 10^{-5}\ (^\circ C)^{-1}$,

$p_1 = 1.\ 10^6$ Pa,

$p_2 = 0.4\ 10^6$ Pa,

$\theta_0 = 30.\ ^\circ C$,

$\vartheta_1 = 400.\ ^\circ C$,

$\vartheta_2 = -10.\ ^\circ C$.

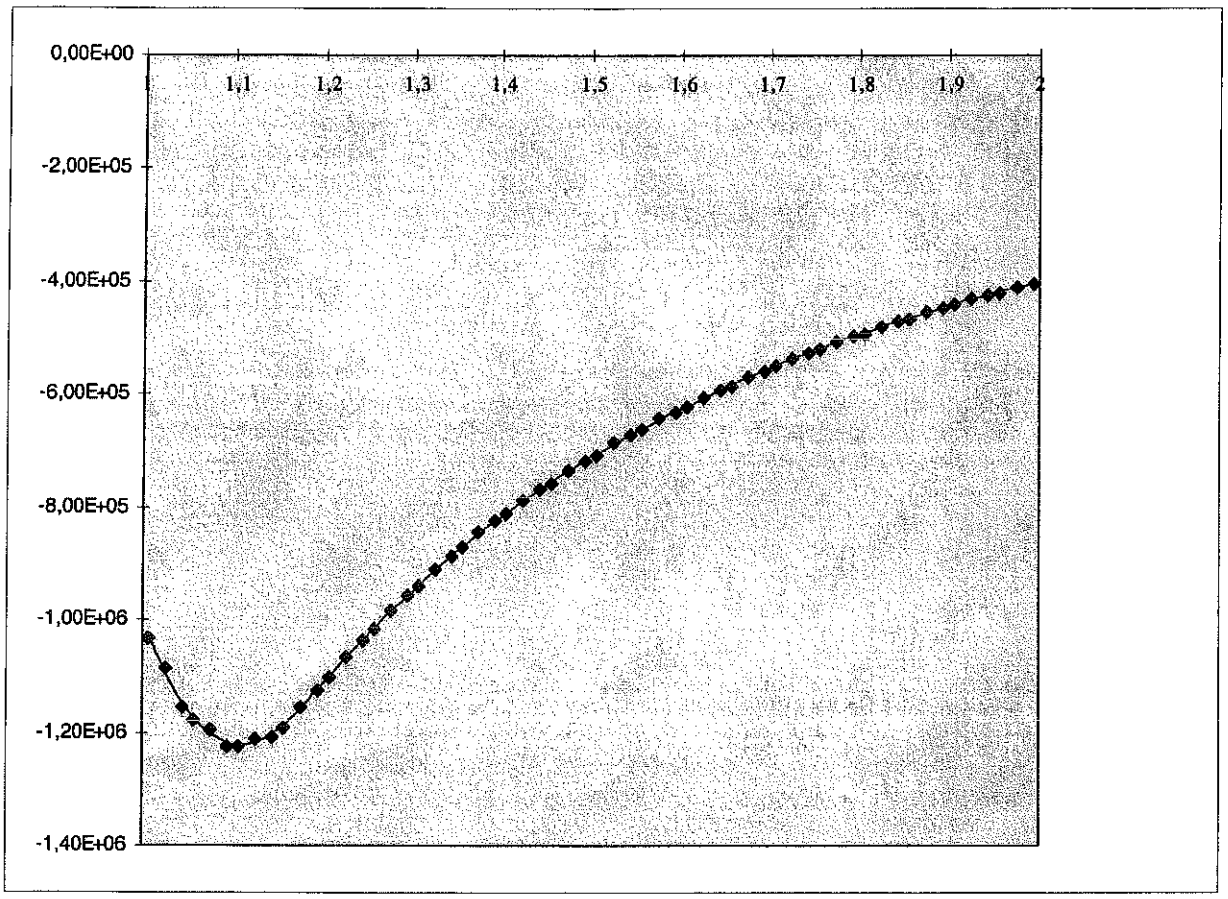

Figure 46. Comparison of radial stress values calculated explicitly and through COMES-NOSA.

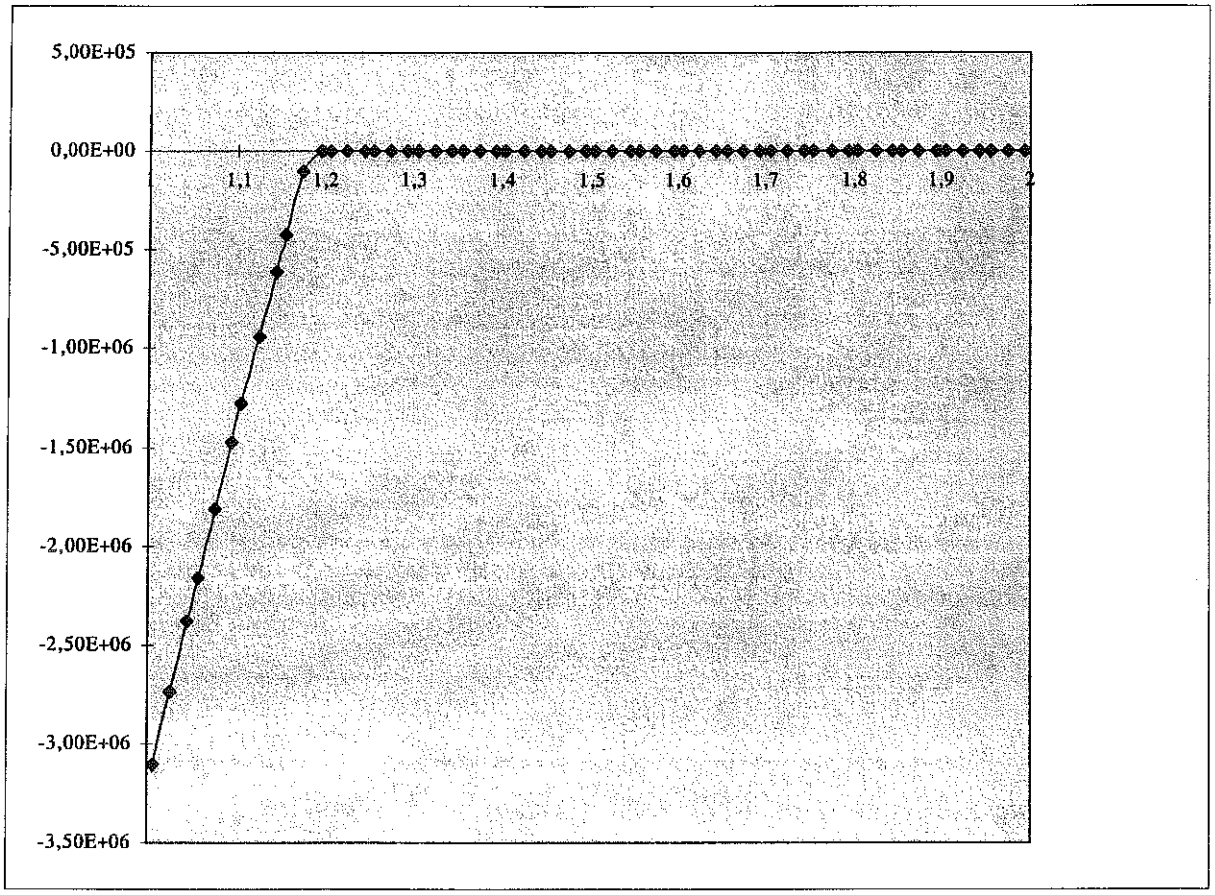

Figure 47. Comparison of tangential stress values calculated explicitly and through COMES-NOSA.

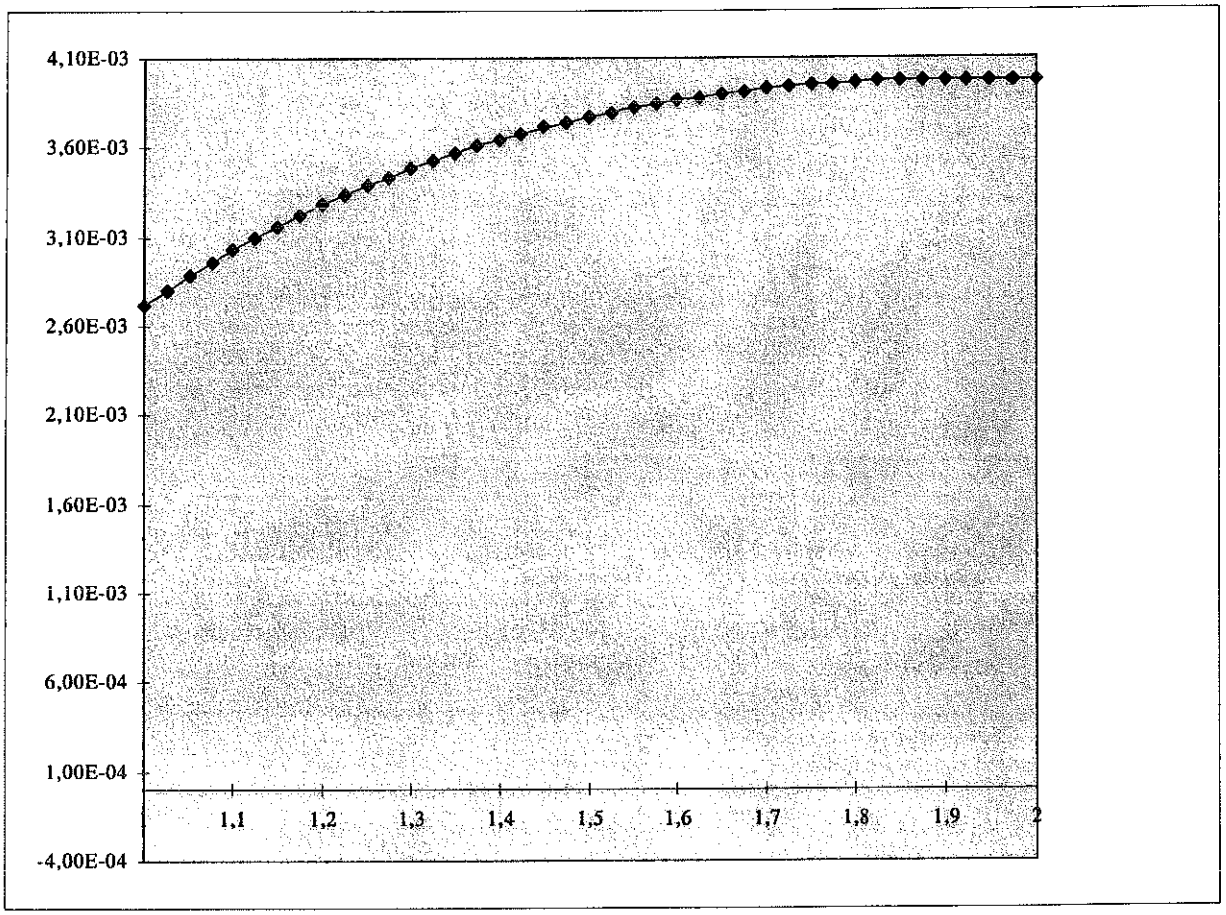

Figure 48. Comparison of radial displacement values calculated explicitly and through COMES-NOSA.

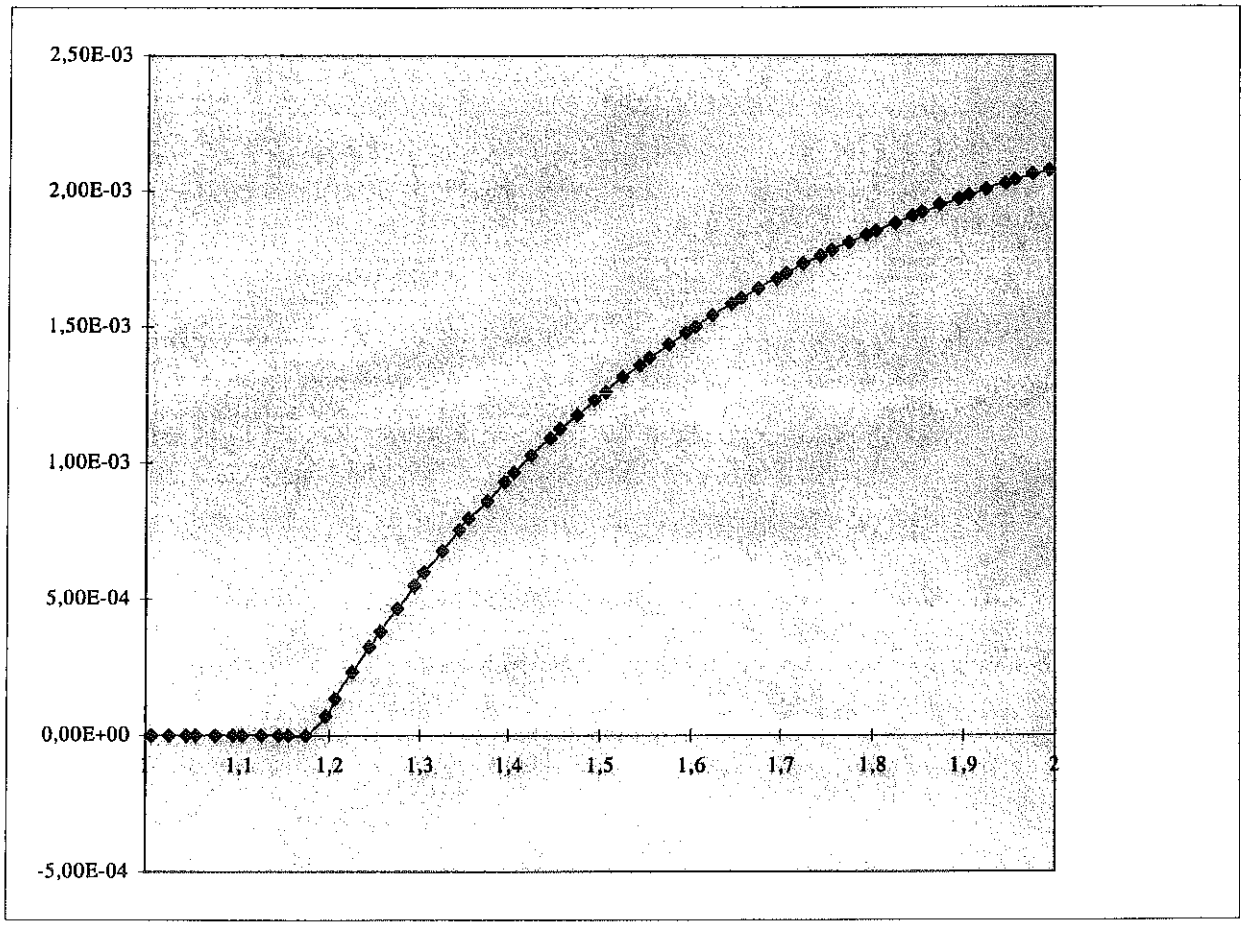

Figure 49. Comparison of tangential inealstc strain values calculated explicitly and through COMES-NOSA.

Bibliography

[1] Padovani C., Pasquinelli G., Zani N., A numerical method for solving equilibrium problems of no-tension solids subjected to thermal loads. *Comput. Methods Appl. Mech. Engrg.* (to appear).

Masonry arch subjected to its own weight and a uniform temperature variation

A circular masonry arch having mean radius of 110 cm and thickness of 20 cm has been discretized with 4800 plane stress elements. The arch, whose springings are fixed, is subjected to its own weight. The reference temperature is $\theta_0 = 30°$ C, and the arch is subsequently brought to a temperature of - 10° C. The elastic constants are independent of temperature and are E = 5000 MPa, $\nu = 0.1$, while the coefficient of thermal expansion is $\beta(\theta) = \alpha(\theta - \theta_0)$, with $\alpha = 1.\ 10^{-5}$ (° C)$^{-1}$. In the first load increment only its own weight was assigned; the temperature variation was introduced over the following four load increments.

Figure 50 and 51 show the lines of thrust, respectively, for the arch subjected to its weight alone and the arch subjected to its own weight plus a temperature variation of - 40 ° C.

The lowering of the crown relative to the first and the fifth increment is 4.07 10^{-3} cm e 1.02 10^{-1} cm, respectively, while the thrust at the springing is 57.6 N in the first case and 54.02 N in the second.

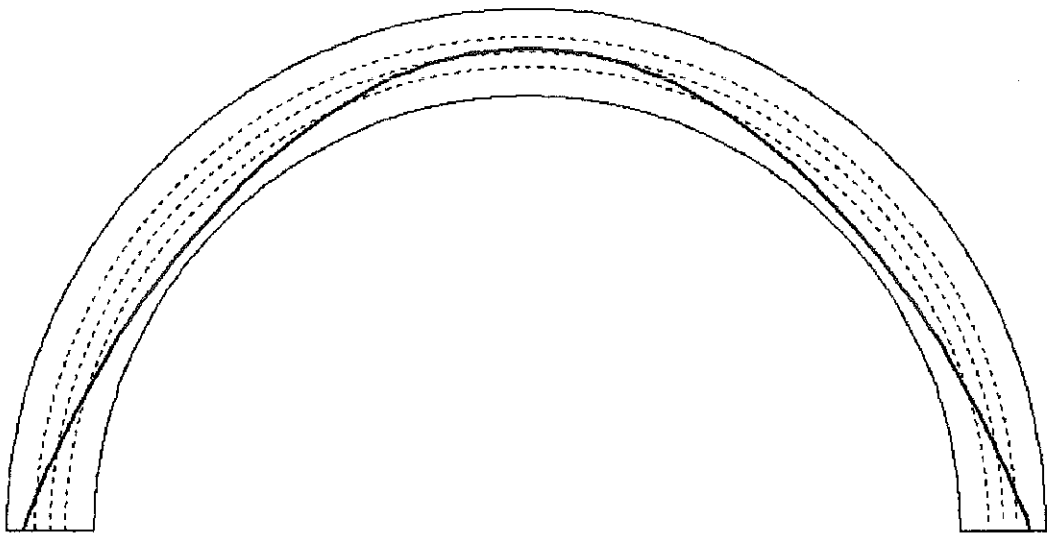

Figure 50. Line of thrust of the arch subjected to its own weight.

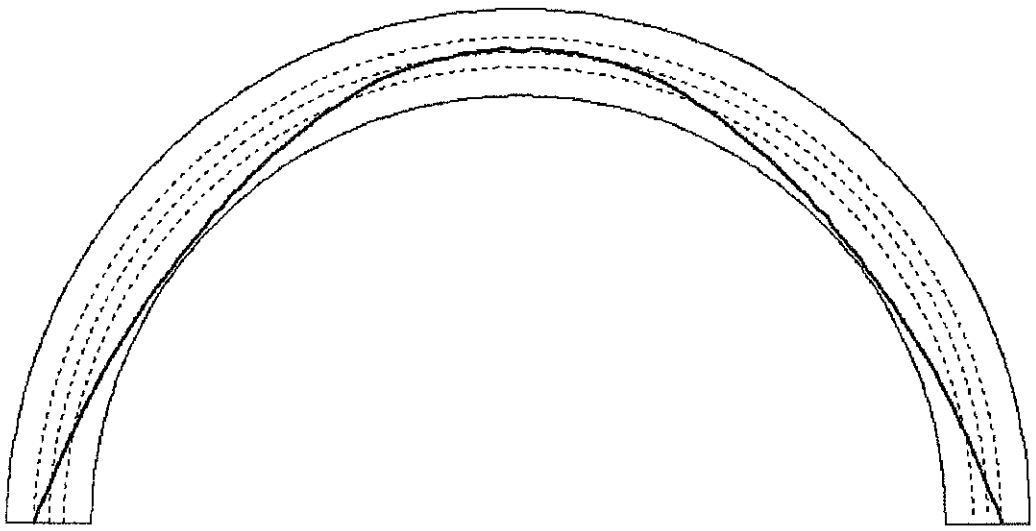

Figure 51. Line of thrust of the arch subjected to its own weight and temperature variation of- 40° C.

Bibliography

[1] Padovani C., Pasquinelli G., Zani N., A numerical method for solving equilibrium problems of no-tension solids subjected to thermal loads. *Comput. Methods Appl. Mech. Engrg.* (to appear).

Converter

A converter used in the iron and steel industry was studied. It is subjected to its own weight and a high thermal gradient. The converter, having axial symmetry, has been discretized using 5068 eight-node axisymmetric elements (figure 52), for a total of 16803 nodes. It is made up of an outer steel casing, plus a wear layer and protective lining, both made of refractory materials, though with different characteristics (figure 53). For the refractories, Poisson's ratio is zero, while Young's modulus varies with temperature. The thermal expansion coefficient $\beta(\theta)$ is temperature-dependent, varying as a linear function for the refractories, but a quadratic one for the steel. The converter is subjected to its own weight and the temperature distribution shown in figure 54. Concerning the boundary conditions, we have imposed symmetry conditions and assigned nil axial displacements to the cylindrical part of the converter (figure 51) in correspondence to the suspension trunnions. Two thermo-mechanical analyses have been carried out: one, considering the refractory to be a material not withstandind tension, the other, modelling the refractory as linear elastic. In both the cases, the steel has been assumed to be a linear elastic material. The results of the analyses have been compared in order to reveal any differences in behaviour.

With regard to the stress field, the regions subjected to tensile stresses in the linear analysis are characterized by nil stress in the non-linear one. Moreover, although the stress fields in the other regions are essentially equal in the two cases, the maximum compressive stresses in the non-linear case are slightly lower. For comparison's sake, figures 55 and 56 show the deformed configuration superimposed upon the initial one for the two analyses. In the case of non-linear behavior, a greater displacement of the lower part is observed.

Disregarding the filling zones, it can be observed that fractures (figures 57 and 58) are concentrated in the protective layer, and will close up during the operational lifetime of the converter. Thus, the foregoing numerical analysis confirms the converter's safety. Moreover, the presence of fractures near the inner surface and parallel to it can be explained by the so-called "onion peeling" mechanism that every converter exhibits at the beginning of its operation.

Regarding the steel container, the areas subjected to the greatest stresses are located near the lower elbow, under the thick reinforcement ring. The calculated stress levels in this zone show that an elastoplastis analysis would have yielded good results. Despite such simplification, the predictions

have been substantiated. In fact, at the end of their operational lifetime, such converters exhibit the greatest problems precisely in the area of the inferior elbow.

The availability of a constitutive equation suitable to modeling refractory behavior, togheter with the numerical techniques necessary to achieve realistic evaluation of the thermo-mechanical behavior of a steel-manufacturing plant's components contributes to reducing the risks and uncertainties associated to the design and control of such plants themselves.

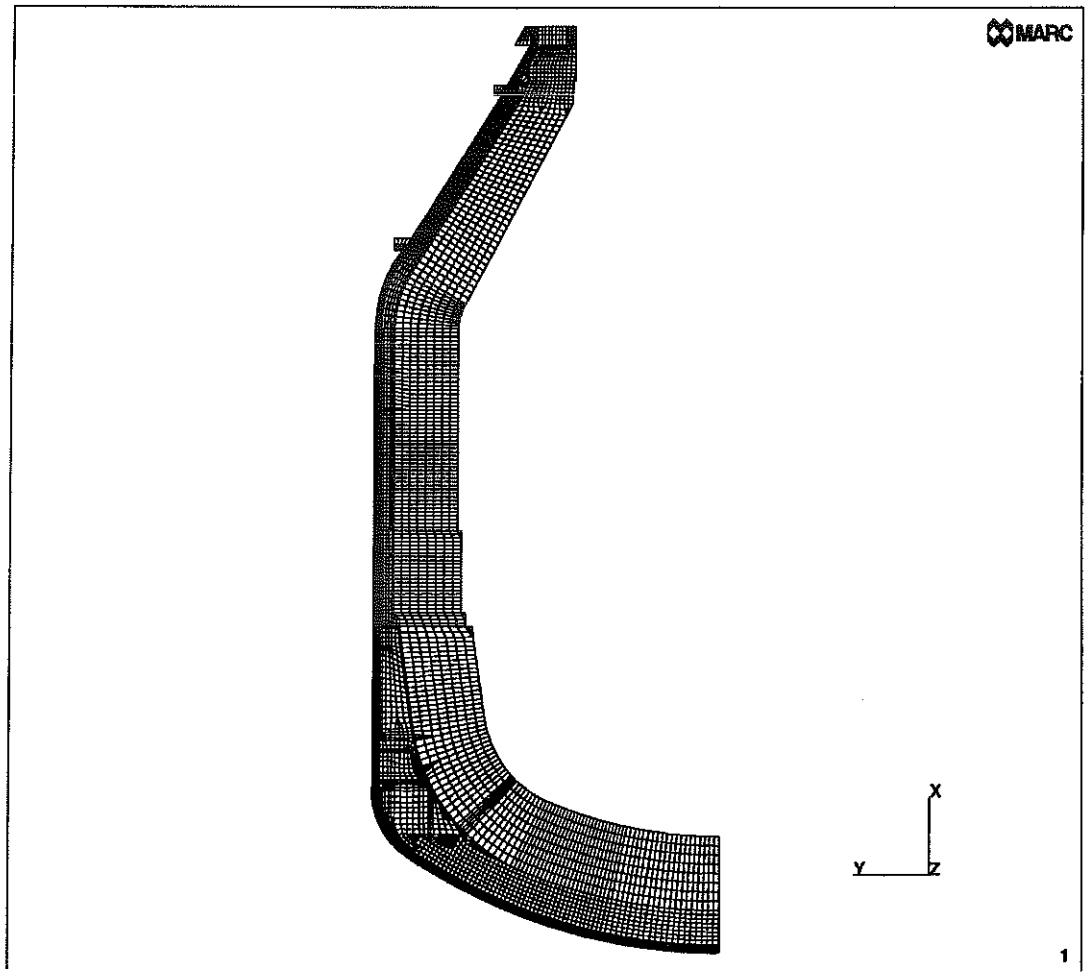

Figure 52. The converter discretized into finite elements.

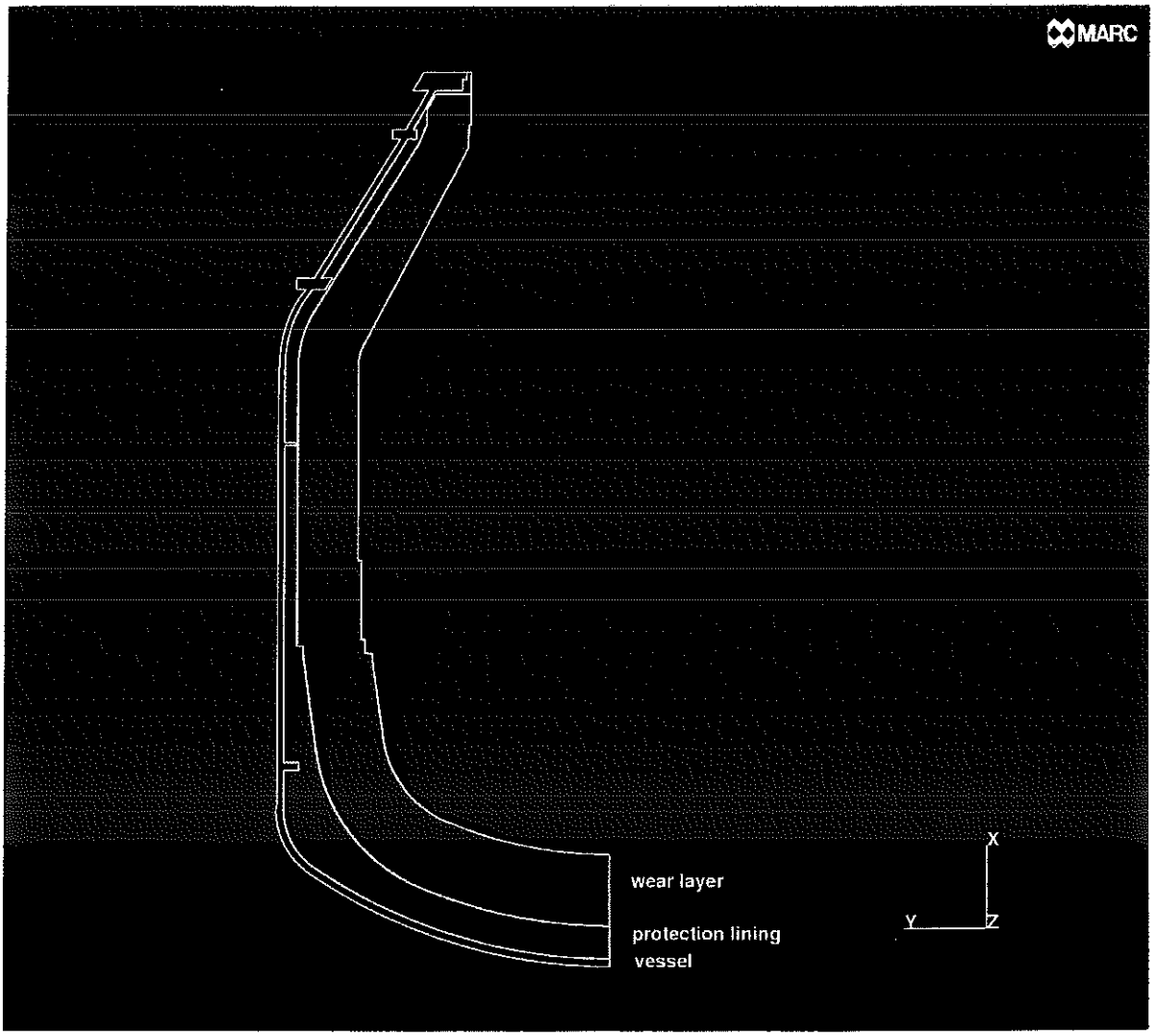

Figure 53. Detail of the converter: wear layer, protective lining and steel casing.

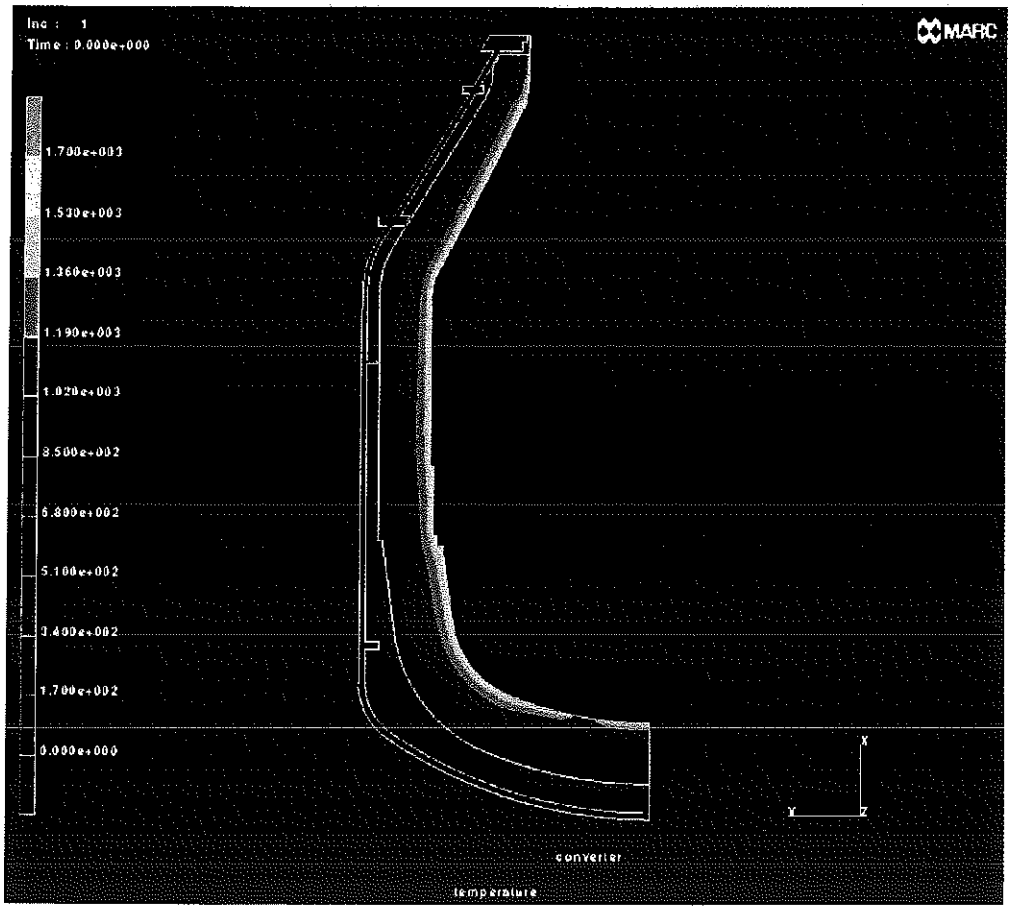

Figure 54. Temperature distribution in the converter.

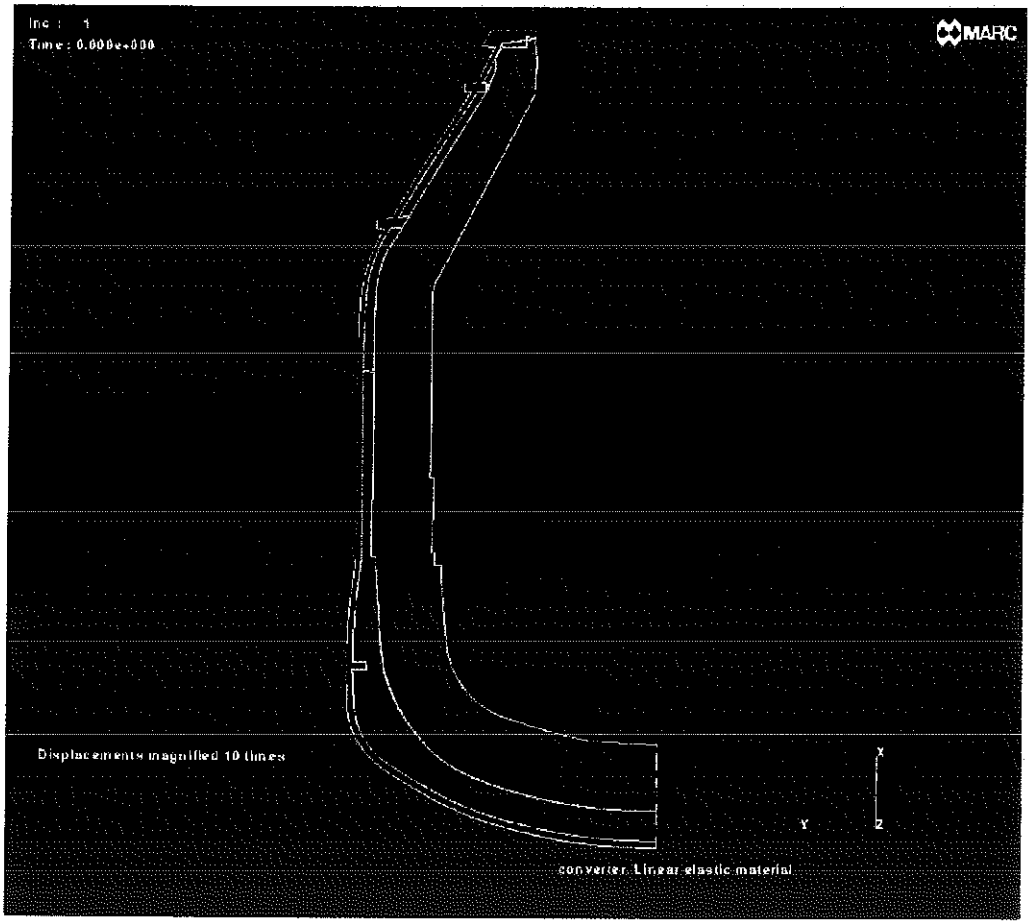

Figure 55. Displacements magnified 10 x, linearelastic case.

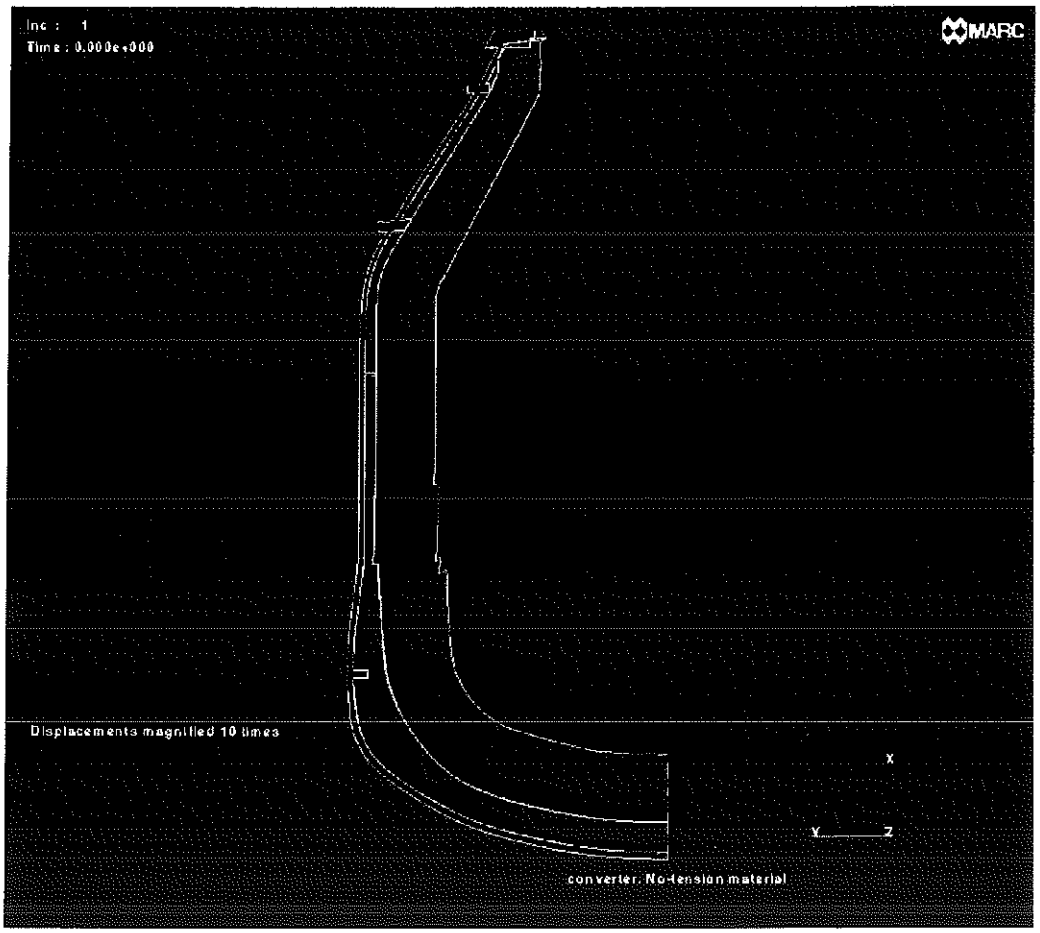

Figure 56. Displacements magnified 10 x, non-linear elastic case.

Figure 57. Fracturing pattern along the meridional planes.

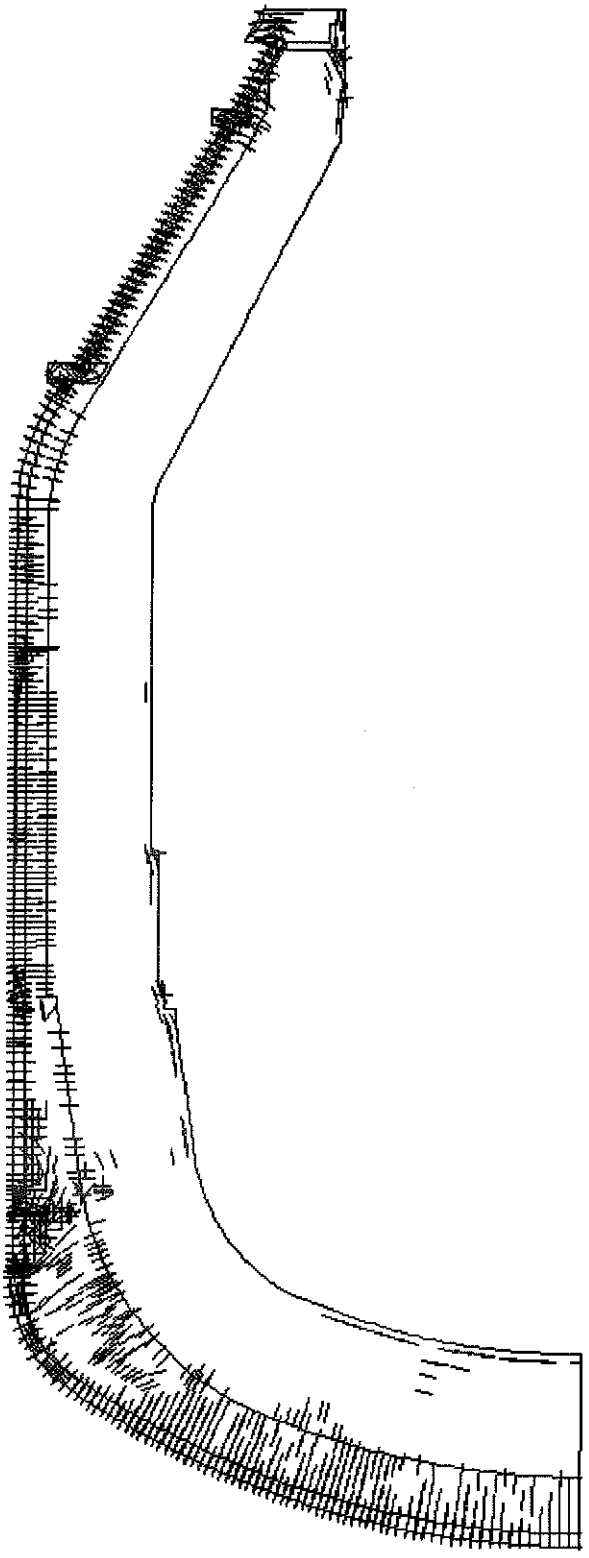

Figure 58. Fracturing pattern along the planes orthogonal to meridians.

Bibliography

[1] Padovani C., Pasquinelli G., Zani N., A numerical method for solving equilibrium problems of no-tension solids subjected to thermal loads. *Comput. Methods Appl. Mech. Engrg.* (to appear).